AGU PUBLICATIONS

Water Resources Research

RESEARCH ARTICLE
10.1002/2016WR019729

This article is a companion to *Torres et al.* [2017], doi:10.1002/2016WR019733.

Special Section:
Concentration-discharge Relations in the Critical Zone

Mixing as a driver of temporal variations in river hydrochemistry: 2. Major and trace element concentration dynamics in the Andes-Amazon transition

J. Jotautas Baronas[1], Mark A. Torres[1,2], Kathryn E. Clark[3], and A. Joshua West[1]

[1]Department of Earth Sciences, University of Southern California, Los Angeles, California, USA, [2]Division of Geology and Planetary Sciences, California Institute of Technology, Pasadena, California, USA, [3]Department of Earth and Environmental Sciences, University of Pennsylvania, Philadelphia, Pennsylvania, USA

Key Points:
- Tributaries of the Madre de Dios River exhibit distinct solute concentrations and concentration-runoff relationships for many elements
- Tributary mixing proportions change systematically with runoff, affecting the concentration-runoff relationships observed downstream
- Mixing effects on concentration-runoff relationships are observed in catchments of 160–28,000 square kilometer area and vary from element to element

Supporting Information:
- Supporting Information S1
- Data Set S1
- Software S1

Correspondence to:
J. J. Baronas,
jotautas.baronas@gmail.com

Citation:
Baronas, J. J., M. A. Torres, K. E. Clark, and A. J. West (2017), Mixing as a driver of temporal variations in river hydrochemistry: 2. Major and trace element concentration dynamics in the Andes-Amazon transition, *Water Resour. Res.*, *53*, 3120–3145, doi:10.1002/2016WR019729.

Received 31 AUG 2016
Accepted 10 MAR 2017
Accepted article online 17 MAR 2017
Published online 17 APR 2017

Abstract Variations in riverine solute chemistry with changing runoff are used to interrogate catchment hydrology and to investigate chemical reactions in Earth's critical zone. This approach requires some understanding of how spatial and temporal averaging of solute-generating reactions affect the dissolved load of rivers and streams. In this study, we investigate the concentration-runoff (C-Q) dynamics of a suite of major (Na, Mg, Ca, Si, K, and SO_4) and trace (Al, Ba, Cd, Co, Cr, Cu, Fe, Ge, Li, Mn, Mo, Nd, Ni, Rb, Sr, U, V, and Zn) elements in nested catchments of variable size, spanning the geomorphic gradient from the Andes Mountains to the Amazon Foreland-floodplain. The major elements exhibit various degrees of dilution with increasing runoff at all sites, whereas the concentrations of most trace elements either increase or show no relationship with increasing runoff in the three larger catchments (160–28,000 km^2 area). We show that the observed main stem C-Q dynamics are influenced by variable mixing of tributaries with distinct C-Q relationships. Trace element C-Q relationships are more variable among tributaries relative to major elements, which could be the result of variations in geomorphology, lithology, and hydrology of the subcatchments. Certain trace metals are also lost from solution during in-channel processes (possibly related to colloidal size-partitioning), which may exert an additional control on C-Q dynamics. Overall, we suggest that tributary aggregation effects should be assessed in heterogeneous catchments before C-Q or ratio-Q relationships can be interpreted as reflecting catchment-wide solute generation processes and their relationship to hydrology.

1. Introduction

The solute chemistry of streams and rivers holds elusive clues about chemical reactions in catchment systems, including mineral dissolution (i.e., chemical weathering), biological and redox transformations, and ion exchange. These reactions determine nutrient supply to ecosystems [e.g., *Berner and Rao*, 1994; *Boyer et al.*, 2006; *Saitoh et al.*, 2008; *Hartmann et al.*, 2014; *Hahm et al.*, 2014; *Frings et al.*, 2016], deliver dissolved material to the oceans [e.g., *Gaillardet et al.*, 1999; *Dürr et al.*, 2011], and influence the transport of contaminants [e.g., *Shiller and Boyle*, 1985; *Meade*, 1996; *Yang and Sañudo-Wilhelmy*, 1998; *Jiann et al.*, 2013]. They also regulate Earth's long-term climate through the consumption of atmospheric CO_2 [*Walker et al.*, 1981; *Berner et al.*, 1983; *Berner*, 1992; *Li and Elderfield*, 2013].

The concentrations of weathering-derived solutes are widely observed to covary with river discharge (referred to as runoff when normalized to catchment area) [e.g., *Hem*, 1948; *Johnson et al.*, 1969; *Godsey et al.*, 2009; *Moon et al.*, 2014]. The origin of these concentration-discharge (C-Q) relationships has been attributed to a variety of processes including source mixing [*Durum*, 1953; *O'Connor*, 1976; *Peters and Driscoll*, 1987; *Derry et al.*, 2006; *Calmels et al.*, 2011; *Kurtz et al.*, 2011; *Peters et al.*, 2014; *Liu et al.*, 2017] and ion-exchange reactions [*Miller and Drever*, 1977; *Clow and Mast*, 2010]. More recently, hillslope-scale solute generation models have been developed and used to interpret C-Q relationships of major elements and, in some cases, to extract intrinsic weathering system parameters in both small and large catchments [*Godsey et al.*, 2009; *Maher*, 2011; *Maher and Chamberlain*, 2014; *Ibarra et al.*, 2016; *Ameli et al.*, 2017]. Largely, these models focus on how the coupling between chemical reactions and fluid flow within hillslopes can lead to covariation between solute concentrations and fluid fluxes.

Available data show significant spatial variations in C-Q relationships [*Walling and Webb*, 1980; *Kirchner et al*., 1993a; *Shand et al*., 2005; *Herndon et al*., 2015; *Godsey et al*., 2009; *Moon et al*., 2014; *Torres et al*., 2015; *Moatar et al*., 2017], consistent with model predictions. This spatial variability means that, in heterogeneous catchments, observed C-Q relationships can be modulated by the mixing of waters sourced from multiple tributary subcatchments with different C-Q relationships [*Creed et al*., 2015; *Moquet et al*., 2015; *Torres et al*., 2017]. Furthermore, for some elements, in-channel chemical reactions [*Neal and Christophersen*, 1989; *Jacobson et al*., 2002] may further act to modulate C-Q relationships. Taken all together, this implies that the C-Q relationships of different elements within the same river system may have different drivers, which can complicate efforts to use models of C-Q relationships to invert for weathering system parameters and to predict behavior of specific elements. That is to say, the interpretation of temporal variations in chemical and isotopic tracers in stream water can be strongly influenced by the aggregation of waters reflecting both spatial [*Kirchner et al*., 1993a; *Kirchner*, 2016a] and temporal [*Kirchner et al*., 1993b; *Kirchner*, 2016b] heterogeneity within the catchment, and these effects need to be considered before using temporal variations to understand solute-generating processes.

Recent efforts in data acquisition and compilation have resulted in a large collection of data on concentration variations with runoff for major elements [e.g., *Godsey et al*., 2009; *Neal et al*., 2013; *Voss et al*., 2014; *Moon et al*., 2014; *Moquet et al*., 2015; *Torres et al*., 2015; *Ibarra et al*., 2016] and a smaller collection of data for trace elements [e.g., *Pettine et al*., 1994; *Shiller*, 1997; *Brezonik et al*., 2003; *Bagard et al*., 2011; *Neal et al*., 2013; *Gaillardet et al*., 2014]. Multiple major and trace elements and their isotopic compositions are also used or currently being developed as paleoenvironment proxies [e.g., *Derry and France-Lanord*, 1996; *Archer and Vance*, 2008; *Misra and Froelich*, 2012; *Moore et al*., 2013; *Georg et al*., 2013; *Pogge Von Strandmann et al*., 2014; *Bruland et al*., 2013], which requires rigorous calibration of their geochemical behavior during critical zone processes. Trace metals can be concentrated in trace mineral phases and are typically sensitive to secondary reactions [e.g., *Murnane and Stallard*, 1990; *Shiller and Mao*, 2000; *Stefánsson and Gíslason*, 2001; *Gaillardet et al*., 2014; *Dellinger et al*., 2015], colloidal versus soluble size fractionation [e.g., *Viers et al*., 1997; *Pokrovsky et al*., 2006; *Bagard et al*., 2011; *Bern et al*., 2011; *Mulholland et al*., 2014; *Ilina et al*., 2016], and nonconservative behavior [e.g., *Cerling and Turner*, 1982; *Mouvet and Bourg*, 1983; *Erel et al*., 1991; *Aucour et al*., 2003; *Mulholland et al*., 2014; *Gaillardet et al*., 2014; *Guinoiseau et al*., 2016]. As such, trace element C-Q dynamics can yield useful information about processes that may not be apparent from major element C-Q relationships alone, including the effects of spatial heterogeneity, tributary mixing, and in-channel chemical reactions. However, little work to date has explored trace element C-Q dynamics systematically and assessed how aggregation effects might influence the use of trace elements as hydrochemical proxies.

In this study, we investigate aggregation effects on major and trace element C-Q relationships in four nested catchments along the Andes-Amazon geomorphic gradient. *Torres et al*. [2015] presented major element data from these sites, showing that C-Q relationships vary systematically from high to low elevation, and raised possible hypotheses for this variation, favoring a role for hillslope mineral and fluid residence times based on a systematic trend in C-Q relationships with catchment slope angles. Here we revisit the possible mechanisms for generating variable C-Q relations at these sites in light of our new trace element data and an accompanying tributary mixing framework. We particularly focus on the role of mixing of heterogeneous sources, a possibility raised by *Torres et al*. [2015] and considered in more detail in a companion paper [*Torres et al*., 2017]. To do this, we utilize coupled C-Q measurements in two small nested Andean catchments and a water and solute mixing model based on conservative tracers δD, Na, and Cl in the larger Madre de Dios River system (model development is described in *Torres et al*. [2017]).

2. Methods

2.1. Study Sites

The primary sites for which concentration-runoff data were collected in this study are four nested catchments located in Peru. These sites span a geomorphic gradient from the Andes Mountains to the Amazon Foreland-floodplain (Table 1, Figure 1). Additional tributaries were also sampled across the study region. The major element concentration-runoff data at the four nested catchments were presented by *Torres et al*. [2015] and the acid and alkalinity sources were apportioned by *Torres et al*. [2016], from whom we borrow

Table 1. Study Site Details

Site	River	Data[a]	Sampling Dates	Latitude	Longitude	Catchment Area (km^2)	Median Elevation (m)	Elevation Range (m)
Andes								
R2250E	Alipachanca	CL	2016/5	−13.1630	−71.5891	35.4	3250	2271–3933
R2250W	Huallpayuncha	CL	2016/5	−13.1629	−71.5895	14.6	3224	2272–3897
Mountain-1 (Wayqecha)[b]	Kosñipata	CQ, CL	2010/1 to 2011/4, 2016/5	−13.1616	−71.5889	50	3242	2262–3933
Mountain-2 (San Pedro)[b]	Kosñipata	CQ, CL	2010/1 to 2011/2, 2015/10	−13.0579	−71.5450	161	2795	1360–4000
Transition								
Mountain-front (MLC)[b]	Alto Madre de Dios	CQ, MM, CL	2010/2 to 2010/12, 2016/5	−12.7901	−71.3903	6,025	1830	452–5496
Manu-MdD confluence	Alto Madre de Dios (Trib. A)[c]	MM	2013/3, 2013/8	−12.2749	−70.9326	7,233	1454	279–5496
Lowlands (Mixed Drainage)								
Manu-MdD confluence	Manu (Trib. B)[c]	MM	2013/3, 2013/8	−12.2722	−70.9345	13,449	430	279–3694
Chiribi-MdD confluence	Chiribi (Trib. C)[c]	MM	2013/3, 2013/8	−12.4950	−70.5912	1,277	369	248–1175
Colorado-MdD confluence	Colorado (Trib. D)[c]	MM	2013/3, 2013/8	−12.6044	−70.4062	3,674	392	234–4252
Foreland-floodplain (CICRA)[b]	Madre de Dios	CQ, MM, CL	2010/2 to 2010/9, 2013/3, 2013/8, 2016/5	−12.5798	−70.0963	27,830	445	219–5496

[a]CL = colloid data, CQ = concentration-runoff data, and MM = mixing model data.
[b]Field stations used as site names in *Torres et al*. [2015] are given in parentheses. MLC = Manu Learning Center.
[c]Tributary labels (A–D) used in the companion paper [*Torres et al*., 2017] are given in parentheses.

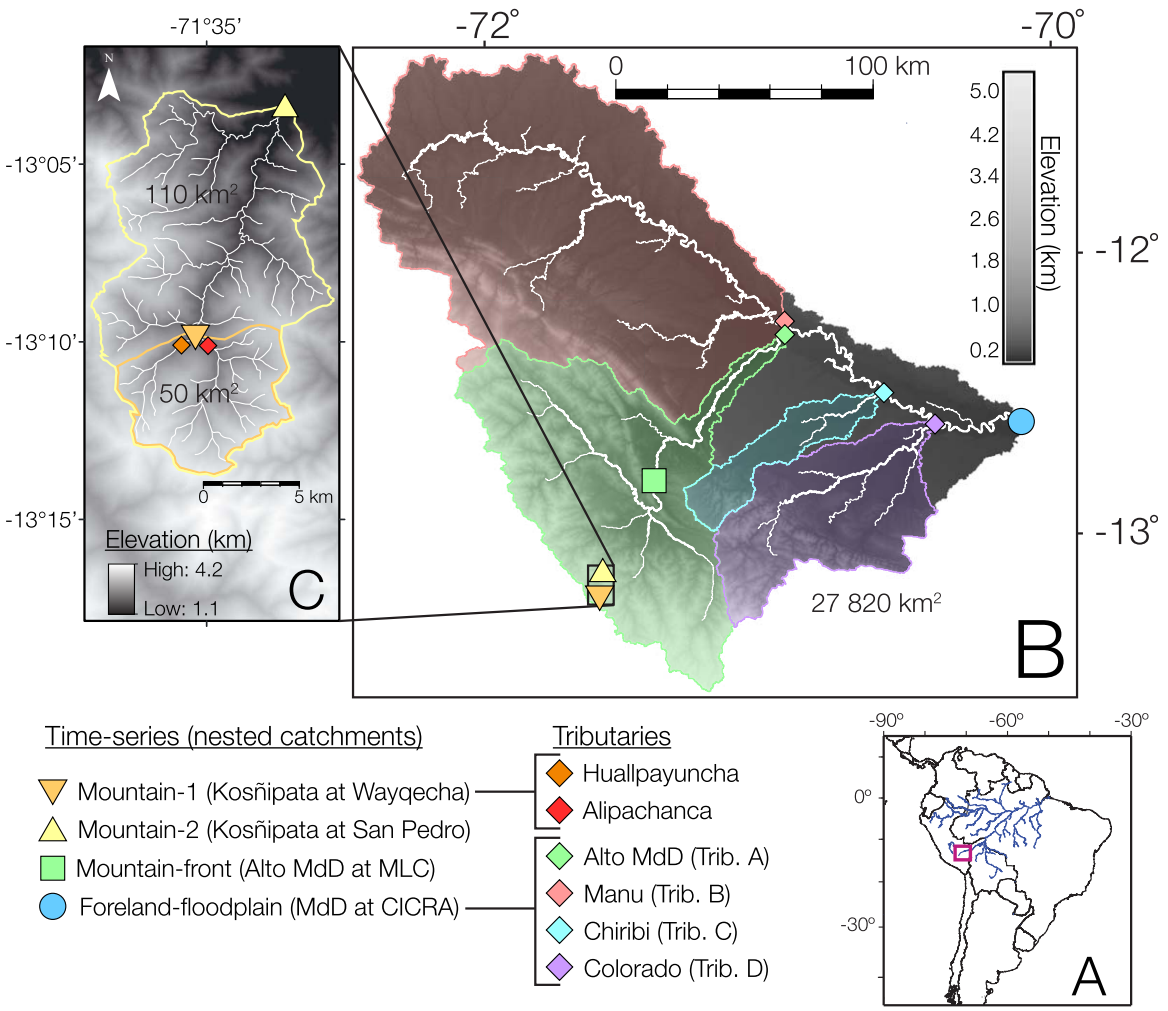

Figure 1. Map of study area. (a) The location of Madre de Dios catchment in the context of the Amazon basin. (b) The whole Madre de Dios catchment draining at the Foreland-floodplain site. (c) The Mountain-1 and Mountain-2 catchments in more detail. MdD = Madre de Dios; MLC = Manu Learning Center.

the site naming convention. Note that samples from the Alto Madre de Dios River used in this study (see Figure 1) include time series samples from the Mountain-front site at Manu Learning Center (MLC) [*Torres et al*., 2015, 2016] as well as additional samples collected further downstream, just above the confluence with the Manu River, and used for constraining tributary mixing [*Torres et al*., 2017].

The Andean (Mountain-1 and Mountain-2) catchments are primarily underlain by Paleozoic (450 Ma) metasedimentary mudstones with some carbonate cements [*Carlotto Caillaux et al*., 1996; *Torres et al*., 2016]. The Mountain-2 catchment also contains a minor Paleozoic felsic plutonic unit (21% of area) [*Carlotto Caillaux et al*., 1996; *Clark et al*., 2013]. The Mountain-front catchment lithology is composed of Paleozoic metasedimentary rocks, Paleozoic plutonic rocks, and Paleozoic marine sedimentary rocks [*Mendívil Echevarría and Dávila Manrique*, 1994; *Carlotto Caillaux et al*., 1996; *Vargas Vilchez and Hipolito Romero*, 1998; *INGEMMET*, 2013]. The Foreland-floodplain is largely underlain by sediments shed from the Andes with additional contributions from Cretaceous marine sediments and Cenozoic continental deposits [*Mendívil Echevarría and Dávila Manrique*, 1994; *Carlotto Caillaux et al*., 1996; *Vargas Vilchez and Hipolito Romero*, 1998; *INGEMMET*, 2013]. Previous studies have classified soils within the Mountain-1 and Mountain-2 catchments as histic Lithosol and umbric Gleysol, respectively, with well-developed (10–20 cm) organic surface layers, whereas Foreland-floodplain soils are typically Ultisols with very little organic matter accumulation [*Girardin et al*., 2010; *Zimmermann et al*., 2012].

The water budgets of the Andean catchments were previously investigated in detail by *Clark et al*. [2014]. During the main study period (2010–2011), annual rainfall was 2519 ± 335 and 3112 ± 414 mm/yr for the Mountain-1 and Mountain-2 catchments, respectively, slightly above the long-term average (based on TRMM and rainfall gauge data) [see *Clark et al*., 2014]. Precipitation in the Foreland-floodplain ranges from 2600 to 3500 mm/yr, with mean values between 2700 and 3000 mm/yr, depending on location [*Lambs et al*., 2012].

2.2. Sample Collection

We have measured trace element concentrations on a subset of samples previously used by *Clark et al*. [2014] and *Torres et al*. [2015, 2016]. Time series samples were collected throughout 2010 and early 2011 into clean polypropylene (PP) bottles, after filtering on-site with a 0.2 μm porosity nylon filter. Additional tributary samples were collected (one sample for each tributary shown in Figure 1) moving downstream over a period of 3 days in both March and August 2013 (these samples were used in the tributary mixing model and are equivalent to the majority of samples also analyzed by *Torres et al*. [2017]) and again in May 2016 (to determine size-partitioning). These tributary samples were collected in clean plastic bags (2013) or plastic syringes (2016) and filtered through 0.2 or 0.45 μm porosity polyethersulfone (PES) filters into polyethylene or polypropylene bottles within 24 h of collection. For all collection periods, aliquots for cation and trace metal analyses were acidified with trace clean HNO_3 or HCl, and separate aliquots for anion and water isotope analyses were left unacidified. Subsets of the samples collected in May 2016 were additionally filtered through 0.02 μm Anotop syringe filters immediately upon collection and also acidified for trace element analysis. In the following text, we refer to the 0.2 or 0.45 μm filtrate as the "bulk dissolved" fraction and the 0.02 μm filtrate as the "soluble" fraction.

Discharge was measured at each of the nested catchment sites as described by *Clark et al*. [2014] and *Torres et al*. [2015]. Briefly, river level and velocity were monitored manually at all sites and converted to discharge using a rating curve. A total of 28, 22, 20, and 11 points were used for the rating curve at the Mountain-1, Mountain-2, Mountain-front, and Foreland-floodplain catchments, respectively. For the Mountain-2 site, river level was also monitored with a water level logger that recorded river level measurements every 15 min. Discharge corresponding to the wet and the dry season samples used in the tributary mixing model at the Foreland-floodplain site was measured using Acoustic Doppler Current Profiler (ADCP) [*Admiraal and Demissie*, 1996] instruments (RD1 Sentinel in March 2013 and SonTek M9 in August 2013).

2.3. Analytical Procedures

Major and some minor solutes were previously analyzed by *Torres et al*. [2015]. Briefly, Na, K, Mg, Ca, Si, Li, and Sr concentrations were measured using an Agilent Microwave Plasma-Optical Emission Spectrometer (MP-OES). Sulfate and chloride concentrations were measured on the unacidified aliquot with a Metrohm

Ion Chromatograph equipped with a Metrosep A4/150 column and conductivity suppression. Precision and accuracy were assessed by analyzing ION-915 (Environment Canada) certified reference material interspersed with samples. Reproducibility of replicate analyses was better than 5% (1σ) for all analytes.

Trace element data were acquired as part of this study. Trace elements were analyzed using a Thermo Scientific Element 2 inductively coupled plasma mass spectrometer (ICP-MS). External calibration curves were used along with signal normalization using an internal Indium standard. The accuracy and precision were determined by replicate analyses of SLRS-5 (National Research Council Canada) and TMDA-51.4 (Environment Canada) certified reference materials. Analytical precision ranged from 1 to 8% (1σ), depending on the element. SRM recoveries ranged from 90 to 110%, always within the certified uncertainty range, where available. Germanium concentrations were measured using isotope dilution hydride generation ICP-MS, utilizing the method developed by *Mortlock and Froelich* [1996] and modified by *Baronas et al.* [2016]. The accuracy and precision based on multiple replicates of NIST-3120a and internal river water standards were better than 5%.

2.4. Data Analysis

2.4.1. Concentration-Runoff Regression Analysis

The relationship between major solute concentrations and runoff, at least over the range of most commonly observed runoff values, can be approximated with power law relationships [*Godsey et al.*, 2009; *Moon et al.*, 2014; *Torres et al.*, 2015]:

$$C = a \times Q^b \tag{1}$$

where C is the dissolved concentration of the element of interest, Q is discharge (volume per time) or area-normalized runoff (length per time), and a and b are fitted parameters. The b exponent describes the steepness and the curvature of the C-Q relationship. The data presented below show that, unlike major solutes, many trace element concentrations do not exhibit clear relationships with runoff, consistent with observations in other studies of riverine trace element concentrations [e.g., *Kirchner and Neal*, 2013]. Therefore, in these cases, a power law regression model is not necessarily more descriptive than, for example, a linear regression model. However, in those cases where trace element concentrations do show significant relationships with runoff (as indicated by their p-values), the power law in general provides a better fit than a linear model (not shown), as indicated by higher degrees-of-freedom adjusted R^2 values. For this reason, and for the ease of comparison between different elements, we fit all solute C-Q relationships with a power law model as in equation (1). The fit parameters and the degrees-of-freedom adjusted R^2 values were extracted using the Curve Fitting Toolbox available in Mathworks MATLAB R2016a software. The correlation p-values for testing the null-hypothesis (i.e., that there is no relationship between C and Q) were extracted using MATLAB's *corrcoef* function. Adjusted R^2 is corrected for degrees-of-freedom in the fit model according to the following formula:

$$Adj.R^2 = 1 - (1 - R^2)\left(\frac{n-1}{n-m-1}\right) \tag{2}$$

where n is the number of data points (samples) in the regression and m is the number of fitting parameters ($m = 2$ for both linear and power law fits). This formulation can sometimes yield negative adj. R^2 values, either when unadjusted R^2 is very close to zero and/or when n is small. Functionally, all adj. $R^2 \leq 0$ values are equivalent and imply no statistical correlation between the regressed variables.

2.4.2. Correlation Analysis

The correlation of the analyzed solutes with runoff (C-Q) and with each other (C-C) was assessed by calculating statistical goodness of fit parameters (R and p-values) for regression trends between all variables (i.e., runoff and concentration of each solute). The trace element concentrations were measured only on a subset of the samples for which major element data were available, so this analysis was carried out on the samples which had the largest number of solutes measured. Additionally, certain trace elements which had lower data density (for example, due to a number of concentrations below the detection limit; see supporting information Table S2) were excluded from this analysis. For consistency with C-Q power law fits discussed elsewhere in this study, all C-Q correlation coefficients were calculated after log-log transformation. All C-C correlation coefficients were calculated in linear space. All variables included in the analysis (runoff and solute concentrations) were normalized to have means of 0 and standard deviations of 1 using MATLAB's

zscore function. The covariance matrices were then calculated using MATLAB's *cov* function and *p*-values using the *corrcoef* function.

2.4.3. Foreland-floodplain Tributary Mixing Model

A tributary mixing model was built to estimate the fraction of discharge and solute fluxes contributed by four main tributaries of the Madre de Dios catchment prior to the Foreland-floodplain site (Figure 1). The methodology and the results of water discharge mixing calculations are described in detail in the companion paper by *Torres et al*. [2017]. Briefly, we utilize the distinct water isotope ratios and Na and Cl concentrations of the various tributaries in the larger Madre de Dios catchment (Figure 1) to calculate the fractional contribution of each tributary to the total water flux at the Foreland-floodplain site during the wet and the dry season. Uncertainty in our mixing model analysis arises from measurement uncertainty as well as storm events that occurred during sampling, which modified the chemical compositions and discharges of some tributaries. The overall uncertainty is assessed using a Monte Carlo approach, where each tributary's composition is selected randomly from within analytical uncertainty and the calculation is repeated 1000 times. Each set of water flux values is then multiplied by solute concentrations (also randomly selected from within analytical uncertainty) 1000 times for storm and nonstorm conditions each, resulting in 2 million individual solute flux calculations for each analyzed element. The model results are then optimized by ensuring that the calculated Na and Cl concentrations match those measured at the Foreland-floodplain site, typically retaining about 10–30% of the calculated values. With the chosen number of repeated calculations, the median and the confidence intervals of each calculated flux are highly reproducible between different model runs. In this study, we applied this model (as developed in *Torres et al*. [2017]) to the extended suite of major and trace elements.

2.4.4. Mineral Saturation Calculation

The calculation of mineral saturation indices was performed for several river water samples collected during low and high runoff using Geochemist's Workbench Edition 11.0.5. Saturation Index is defined as $SI = \log (IAP/K_{sp})$, where *IAP* is the ion activity product of relevant dissolved species and K_{sp} is the equilibrium solubility product of a given mineral. We used average annual temperature at each given site. Dissolved oxygen concentration was assumed to be at saturation for the given temperature, and bicarbonate concentration was calculated by assuming charge balance of the dissolved major ions. There is no pH data available for the samples discussed here, but separate measurements of Madre de Dios water in May 2016 yielded pH values between 6 and 7. The thermodynamic calculation was therefore done for all samples twice, assuming pH of either 6 or 7. The choice of pH had a relatively small effect on most calculated SI values. The parameters used in calculating saturation indices and the results are given in supporting information Table S5.

3. Results

The ranges of bulk dissolved ($<$0.2 μm filtrate) element concentrations and runoff measured at each of the four time series sites are presented in Table 2 and Figure 2. The individual sample data are given in supporting information Table S2. Discharge measurements and major element, Li, and Sr concentrations were reported previously by *Torres et al*. [2015] and are used for discussion purposes alongside the trace element data presented in this study. For the readers' convenience, the data from *Torres et al*. [2015] are also included in supporting information Table S2.

Trace metal (note: all trace elements measured in this study are metals, and therefore the two terms, metal and element, will be used interchangeably) concentrations in the Kosñipata and Madre de Dios Rivers range from pmol/L (e.g., U, Ge) to μmol/L (e.g., Fe, Al, Sr, Li), generally consistent with previous observations in other pristine rivers [*Gaillardet et al*., 2014]. As reported by *Torres et al*. [2015], major element concentrations show minor temporal variations, especially at the Andean sites (Figure 2). In contrast, trace metal concentrations are much more variable with time at each site, as well as between the different sites. For some elements, variations span 3 orders of magnitude across the sampled catchments (Figure 2).

3.1. Intersite Variation in Element Concentrations

Different element concentrations show differing intersite behavior along the geomorphic gradient. Elements that show consistently increasing concentrations along the Andes-to-Amazon transition are U, Ge, Mo, V, Cr, Ba, Rb, and K. Concentrations of Na, Ca, Mg, and Sr decrease from Andean sites (Mountain-1 and

Table 2. The Range of Runoff and Element Concentrations Measured in the Time Series Sample Set, Corresponding to Figures 2–5[a]

		Mountain-1 (Kosñipata)	Mountain-2 (Kosñipata)	Mountain-Front (Alto MdD)	Foreland-Floodplain (Madre de Dios)
Major elements	n=	85	58	52	23
Trace elements	n=	32–39	20–38	24–34	22
Runoff (Q)	mm/d	2.2–28.2	1.9–18.6	2.6–14.8	2–7.6
Cl	μmol/L	1.6–15.4	1.4–12.7	6.2–30.9	6.4–59.8
Na	μmol/L	74.8–189.6	53.8–127.7	48.4–110.9	21–171.3
Mg	μmol/L	91–232.2	47.8–119.8	26.5–83.1	18.7–149.3
Ca	μmol/L	115.4–267	73.4–187	48.2–167.8	91.5–500.6
K	μmol/L	3.2–12.6	3.9–23.2	6.2–26.5	9.7–32.4
Si	μmol/L	146.6–302.7	133.4–235.1	100.6–204.9	42.7–246.5
SO_4	μmol/L	193.5–510.9	94–251.7	30.7–126.9	14.3–115.5
Li	μmol/L	1.24–3.26	0.6–1.37	0.14–0.5	0.03–0.3
Sr	μmol/L	0.4–1.03	0.34–0.98	0.22–0.73	0.2–4.46
Al	μmol/L	0.91–5.34	0.18–2.56	0.79–17.81	0.6–3.94
Fe	μmol/L	0.12–2.72	0.02–1.53	0.28–10.01	0.1–2.66
Mn	μmol/L	1.42–5.05	0.03–3.14	0.31–1.81	0.04–0.25
V	nmol/L	0.1–2.4	0.3–2.8	5.6–22	17.4–22
Ba	nmol/L	17–94	14–89	35–557	235–650
Cd	nmol/L	0.13–1.01	0.05–0.6	0.03–1.38	0.02–0.64
Co	nmol/L	22.2–159.6	0.9–66.9	1.7–9.6	0.8–8.2
Cr	nmol/L	0.2–2.42	0.13–3.02	1.38–79.97	1–3.6
Cu	nmol/L	6.9–26.8	1.7–34.7	11.5–75.2	8.2–36.6
Ge	pmol/L	66–130	65–155	110–240	117–208
Mo	nmol/L	0.2–1.2	1.8–5.7	1.4–6.6	3.7–5.8[b]
Nd	nmol/L	0.26–2.85	0.06–4.55	0.22–3.48	0.05–0.97
Ni	nmol/L	66–428	27–179	12.7–31.8	6.6–10.9[c]
Rb	nmol/L	3.05–7.05	8.4–25.6	12.2–29.7	11.1–18
U	pmol/L	11–200	36–329	32–168	55–1028
Zn	nmol/L	51–528	36–493	37–696	35–319

[a]Individual data are given in supporting information Table S2. Alto Madre de Dios River samples are from the Mountain-front (MLC) site.
[b]n = 6.
[c]n = 5.

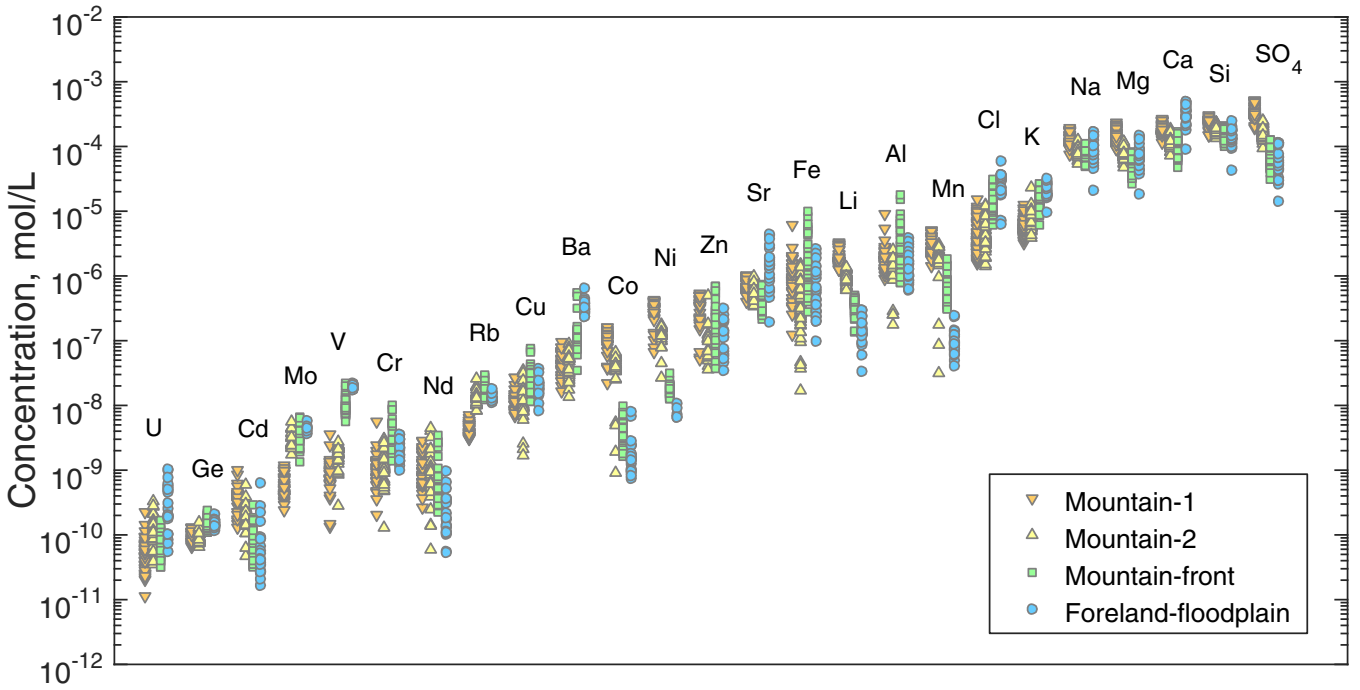

Figure 2. The range of major and trace element concentrations measured at the four time series sites. The elements are sorted from lowest to highest mean concentration at the Mountain-1 site.

Table 3. Concentration-Runoff Power Law Exponents With Uncertainty, and Goodness of Fit[a]

	Mountain-1 (Kosñipata)				Mountain-2 (Kosñipata)				Mountain-Front (Alto Madre de Dios)				Foreland-Floodplain (Madre de Dios)			
	b exp.	2σ	R^2	*p*	*b exp.*	2σ	R^2	*p*	*b exp.*	2σ	R^2	*p*	*b exp.*	2σ	R^2	*p*
Na	−0.35	0.04	0.75	<0.01	−0.26	0.02	0.89	<0.01	−0.34	0.09	0.53	<0.01	−0.75	0.15	0.83	<0.01
Mg	−0.35	0.06	0.60	<0.01	−0.26	0.03	0.86	<0.01	−0.48	0.10	0.70	<0.01	−0.76	0.15	0.84	<0.01
Ca	−0.31	0.05	0.60	<0.01	−0.28	0.02	0.89	<0.01	−0.49	0.10	0.69	<0.01	−0.50	0.16	0.64	<0.01
K	0.00	0.13	−0.01	0.60	0.12	0.17	0.02	0.25	0.04	0.19	−0.02	0.54	−0.41	0.13	0.63	<0.01
Si	−0.13	0.04	0.34	<0.01	−0.15	0.03	0.62	<0.01	−0.24	0.08	0.45	<0.01	−0.46	0.15	0.63	<0.01
Li	−0.42	0.05	0.68	<0.01	−0.22	0.05	0.53	<0.01	−0.30	0.13	0.32	<0.01	−0.72	0.19	0.72	<0.01
Sr	−0.30	0.06	0.48	<0.01	−0.34	0.04	0.85	<0.01	−0.47	0.13	0.56	<0.01	−1.07	0.29	0.75	<0.01
SO_4	−0.36	0.05	0.67	<0.01	−0.24	0.04	0.69	<0.01	−0.63	0.12	0.73	<0.01	−0.83	0.16	0.84	<0.01
Al	0.23	0.38	0.02	0.06	0.41	0.19	0.41	<0.01	0.17	0.75	−0.02	0.62	0.34	0.67	0.01	0.61
Fe	−0.27	0.42	0.01	<0.01	0.45	0.54	0.07	0.07	0.04	0.81	−0.03	0.83	1.08	1.52	0.09	0.30
Mn	−0.36	0.12	0.47	<0.01	0.29	0.18	0.24	0.08	0.18	0.36	0.00	0.60	0.69	0.61	0.20	0.05
V	0.27	0.38	0.04	0.04	0.22	0.13	0.25	<0.01	0.06	0.26	−0.02	0.55	0.03	0.07	0.00	0.34
Cr	0.22	0.43	0.00	0.18	0.06	0.25	−0.02	0.11	−0.23	0.64	−0.02	0.41	0.45	0.37	0.25	0.00
Co	−0.24	0.13	0.26	<0.01	0.31	0.20	0.24	<0.01	0.33	0.30	0.11	0.04	0.16	0.93	−0.04	0.98
Ni	−0.26	0.12	0.30	<0.01	0.12	0.15	0.06	0.12	0.10	0.15	0.02	0.22	n/a	n/a	n/a	n/a
Cu	−0.13	0.18	0.02	0.17	0.07	0.33	−0.03	0.25	0.31	0.40	0.04	0.03	0.20	0.32	0.04	0.09
Zn	−0.50	0.14	0.61	<0.01	0.00	0.62	−0.06	0.52	0.82	0.78	0.12	0.11	0.54	0.90	0.07	0.21
Rb	−0.13	0.11	0.10	0.02	−0.07	0.12	0.01	0.11	−0.02	0.18	−0.03	0.55	−0.18	0.10	0.38	<0.01
Mo	−0.35	0.20	0.22	0.01	−0.38	0.10	0.76	<0.01	−0.61	0.39	0.30	0.01	n/a	n/a	n/a	n/a
Cd	−0.17	0.20	0.04	0.14	0.07	0.22	−0.02	0.20	−0.10	0.49	−0.03	0.27	0.79	1.96	0.01	0.10
Ba	−0.39	0.11	0.54	<0.01	−0.13	0.18	0.02	0.07	0.16	0.59	−0.02	0.28	−0.02	0.26	−0.05	0.67
Nd	−0.44	0.21	0.32	<0.01	4.38	1.72	0.30	<0.01	1.02	0.52	0.27	<0.01	2.93	2.03	0.30	0.02
U	−0.44	0.27	0.18	<0.01	−0.04	0.25	−0.02	0.62	−0.20	0.34	0.01	0.14	−1.16	0.44	0.63	<0.01
Ge	−0.11	0.12	0.06	0.16	0.10	0.08	0.10	<0.01	0.07	0.14	0.00	0.36	0.11	0.13	0.10	0.09

[a] R^2 values are adjusted for the number of degrees-of-freedom in the regression. The values for major elements, Li, and Sr have been previously reported by *Torres et al*. [2015]. Alto Madre de Dios River samples are from the Mountain-front (MLC) site.

Mountain-2) to the Mountain-front but increase again in the Foreland-floodplain. In contrast, SO_4, Cd, and Nd decrease moderately but continuously from Mountain-1 to the Foreland-floodplain, and Mn, Li, Ni, and Co decrease by 2–3 orders of magnitude along the elevation gradient. Cu, Zn, Fe, and Al do not show systematic intersite changes.

3.2. Intrasite Variation in Element Concentrations

The temporal variations in runoff and dissolved element concentrations measured at each given site over a period of 9–16 months are presented in supporting information Figure S1. Subdaily variations (measured over a period of 2–3 weeks in 2010) are presented in supporting information Figure S2. Once again, there is a clear distinction between the major and trace elements. Most of the variability in major element concentrations occurs over seasonal time scales, whereas certain trace element concentrations can change significantly on a time scale of days and sometimes hours (supporting information Figure S1). These differences between elements are further showcased in their concentration-runoff relationships, discussed below. Again, we note that the differences between major and trace element C-Q relationships reported in this study are observed in other riverine data sets [e.g., *Kirchner and Neal*, 2013].

3.3. Concentration-Runoff Relationships

The concentration-runoff (C-Q) relationships of major elements, as well of Li and Sr, were previously discussed in detail by *Torres et al*. [2015]. Briefly, Na, Mg, Ca, Si, Li, Sr, and SO_4 exhibit strong correlation (Adj. $R^2 = 0.3$–0.8; p-values < 0.01; Table 3 and Figure 3) with runoff that indicates various degrees of dilution with increasing runoff (C-Q power law slopes between −1 and 0; termed dilutional-chemostatic). Potassium is the only major element that behaves differently, showing no dilution at the Mountain-1 and Mountain-front sites and possibly a moderate increase at higher runoff at the Mountain-2 site ($p = 0.08$). However, K concentrations are relatively low (3–30 μmol/L across all sites), and appear to behave similarly to Fe and Al, which are considered trace elements in natural waters.

In contrast to the major elements, most trace metals show a much weaker correlation (Adj. R^2 from −0.1 to 0.8; p-values from <0.01 to 0.9) with runoff (Table 3, Figure 3). Almost all trace metals at the Mountain-1 site show a chemostatic-dilutional relationship with runoff that mimics the major elements (i.e., zero to negative

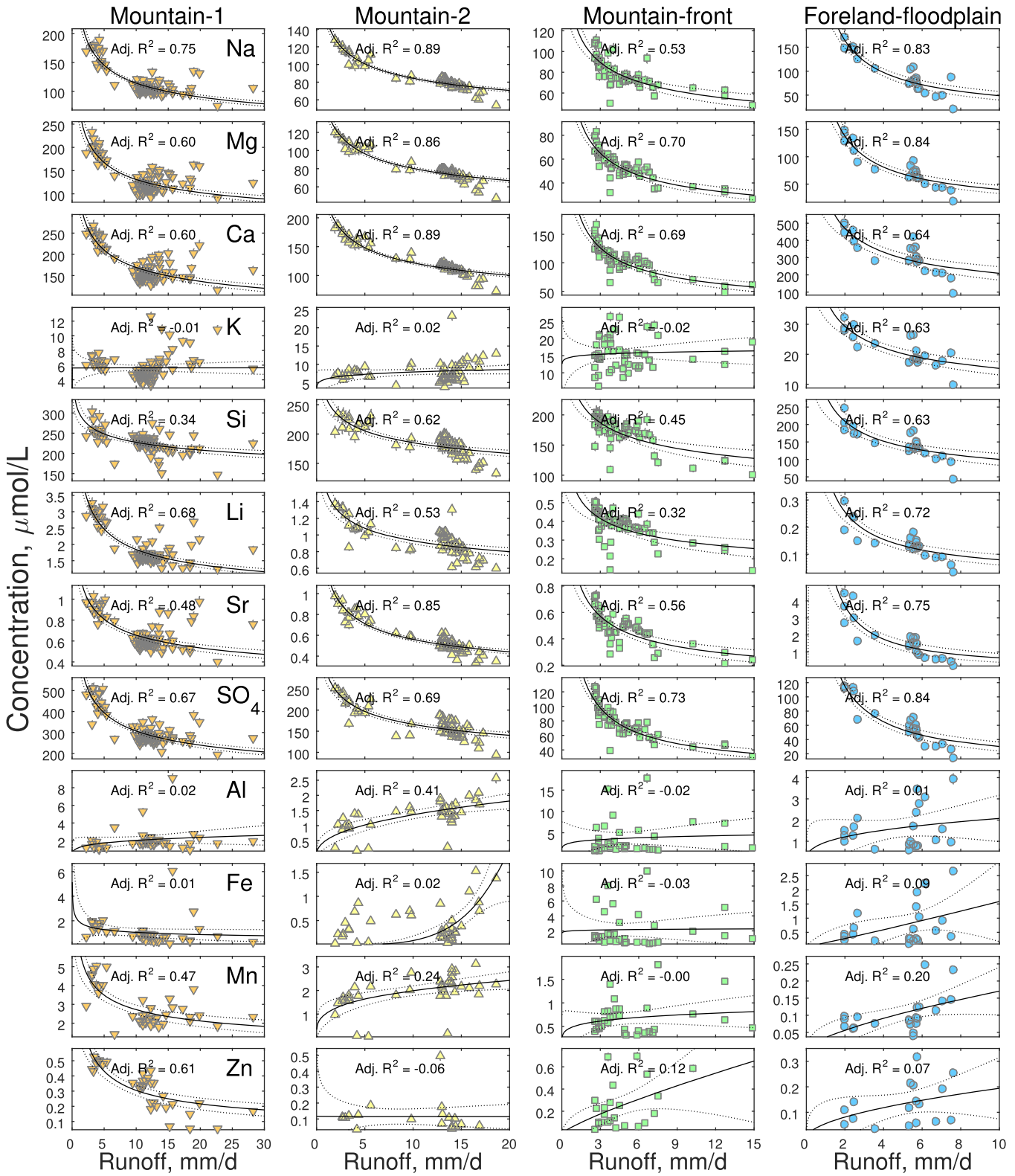

Figure 3. Concentration-runoff relationship of major and trace element concentrations. Solid black line is a power law fit; dashed lines denote 95% confidence interval. Degrees-of-freedom-adjusted R^2 is provided for each fit. Ni and Mo at the Foreland-floodplain site are not fit due to a number of samples below the detection limit and the resulting small number of data points.

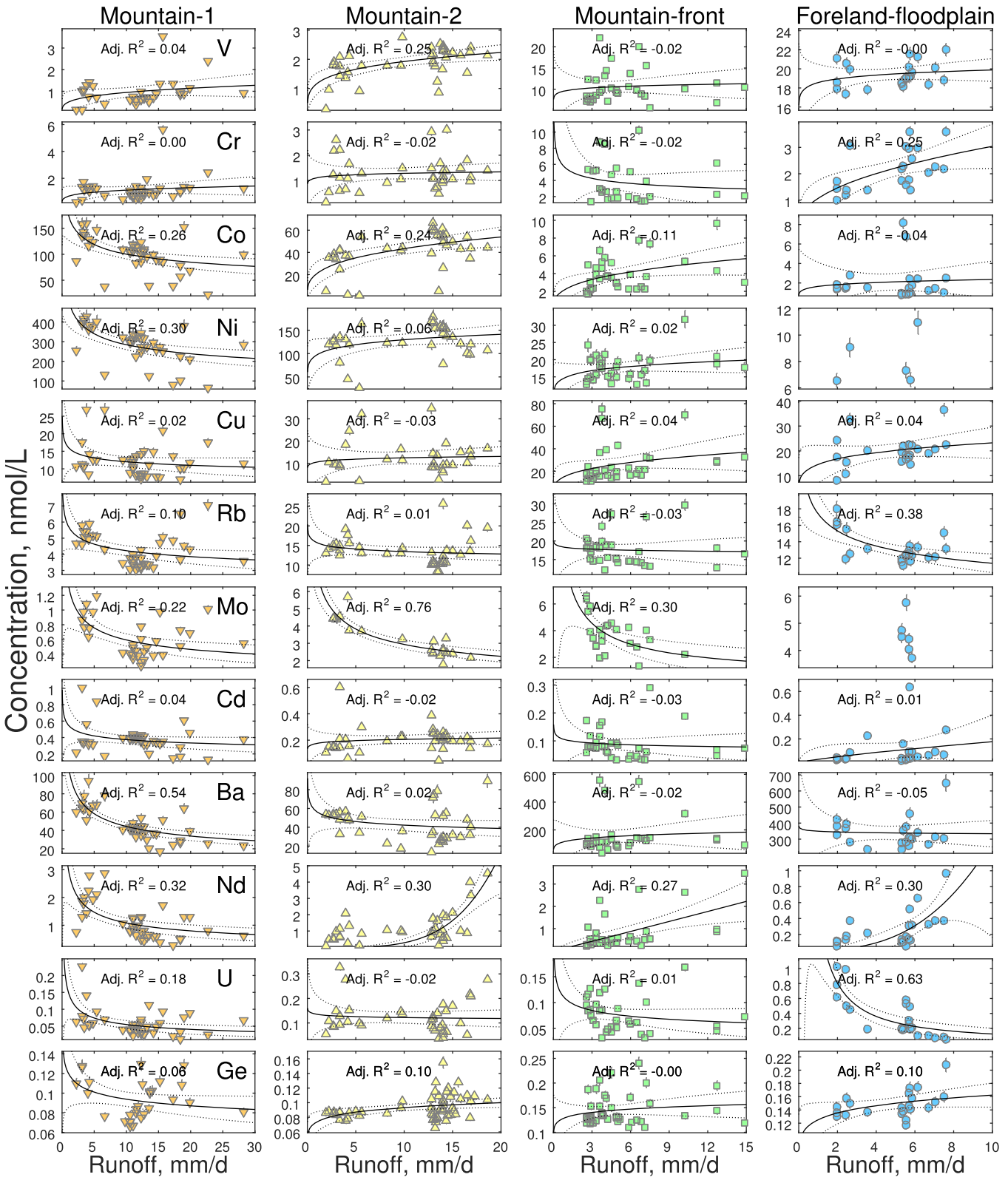

Figure 3. (continued).

b exponents). At the Mountain-2 and Mountain-front sites, most trace elements show either no relationship or a weak positive correlation with runoff (small positive *b* exponents). The contrast between the major and the trace elements is strongest at the Foreland-floodplain site, where major elements show the strongest dilution and several trace elements show the most positive correlation with runoff (large positive *b* exponents; Table 3). A large portion of the trace elements exhibit C-Q relationships that are unlikely to be statistically significant (4, 7, and 11 out of 16 trace elements analyzed at the Mountain-1, Mountain-2, and Mountain-front sites, respectively, have C-Q *p*-values > 0.1 and 6 out of 14 analyzed at the Foreland-floodplain site have *p*-values > 0.1), which may imply chemostatic behavior. However, a number of trace elements show relatively large concentration variations independent of runoff, resulting in large uncertainty of their *b* exponents (Figure 4), which precludes the interpretation of the their C-Q relationships as chemostatic.

In summary, most major elements demonstrate statistically significant dilutional-chemostatic behavior ($-1 < b < 0$, small uncertainty) at all sites, whereas most trace elements exhibit similar negative *b* exponents at the Mountain-1 site but switch to either positive *b* exponents, chemostatic behavior ($b \approx 0$), or no identifiable relationship with runoff (large b uncertainty) at the other sites.

3.4. Correlation Analysis

Figure 5 shows the correlation between runoff and the concentrations of most of the elements measured in this study. Major elements, Li, and Sr are always strongly correlated with each other, except for K, which joins the cluster only at the Foreland-floodplain site. The negative correlation between major elements and runoff becomes stronger (i.e., higher *R* values in Figure 5) with decreasing elevation, as described previously [*Torres et al*., 2015]. Although not as strongly, other trace elements also show negative correlation with runoff and positive correlation with the major elements at the Mountain-1 site. At the other three sites, however, most trace elements are to varying degrees anticorrelated with the major elements and positively correlated with runoff (Figure 5). The correlation of the major elements (including Li and Sr) with each other, the correlation of several of the trace elements with each other (e.g., Al, Fe, Mn, V, Cr, Nd), and the decoupling (anticorrelation) of the two groups becomes stronger with decreasing elevation and increasing catchment area from Mountain-2 to the Foreland-floodplain.

3.5. Soluble Versus Colloidal Size-Partitioning

To better elucidate the controls on river trace element chemistry across the geomorphic gradient, a number of samples were filtered to separate the soluble (also sometimes referred to as the "truly dissolved" fraction and defined here as 0.02 μm filtrate) and the colloidal (defined as the difference between the 0.02 μm and the 0.2 μm filtrates) concentrations at the four time series sites discussed above, as well as the two small Andean rivers joining to form the Kosñipata River at Wayqecha (Table 1, Figure 1).

The results are summarized in Table 4 and Figure 6. The size-partitioning varies from element to element, as well as from site to site. Si is completely soluble within analytical uncertainty at all the sites, in agreement with data from other rivers [e.g., *Pokrovsky et al*., 2006]. Nd is the only element found predominantly in the colloidal phase at all the sites (48–94% colloidal). Fe is also consistently colloidal (77–89%), except for the Andean stream Alipachanca (0%) that has unique chemistry with extremely high soluble concentrations of several trace elements, especially Fe (55 μmol/L). Several streams contributing to Alipachanca are likely to have extremely high Fe concentrations, based on the bright orange color of their suspended load as observed in the field. The Alipachanca is one of the two main tributaries that join to form the Kosñipata River at the Mountain-1 site, which therefore results in the relatively low colloidal Fe at this site (12%).

Rb and V are found predominantly in the soluble phase across all sites. The colloidal Ba fraction ranges from 0 to 19%. Colloidal Mn and Co partitioning varies distinctly between study sites: the colloidal fraction is low in the Andean streams (0–5%) but increases up to 96% and 73%, respectively, in the Foreland-floodplain. U displays the opposite behavior, with the colloidal fraction up to 100% in the Andean streams but almost entirely soluble partitioning in the Foreland-floodplain (Table 4 and Figure 6).

4. Discussion

The theory for mixing of tributary C-Q relationships is outlined in more detail in the companion paper [*Torres et al*., 2017] and is briefly reviewed here. Let us consider two hypothetical tributaries that mix prior

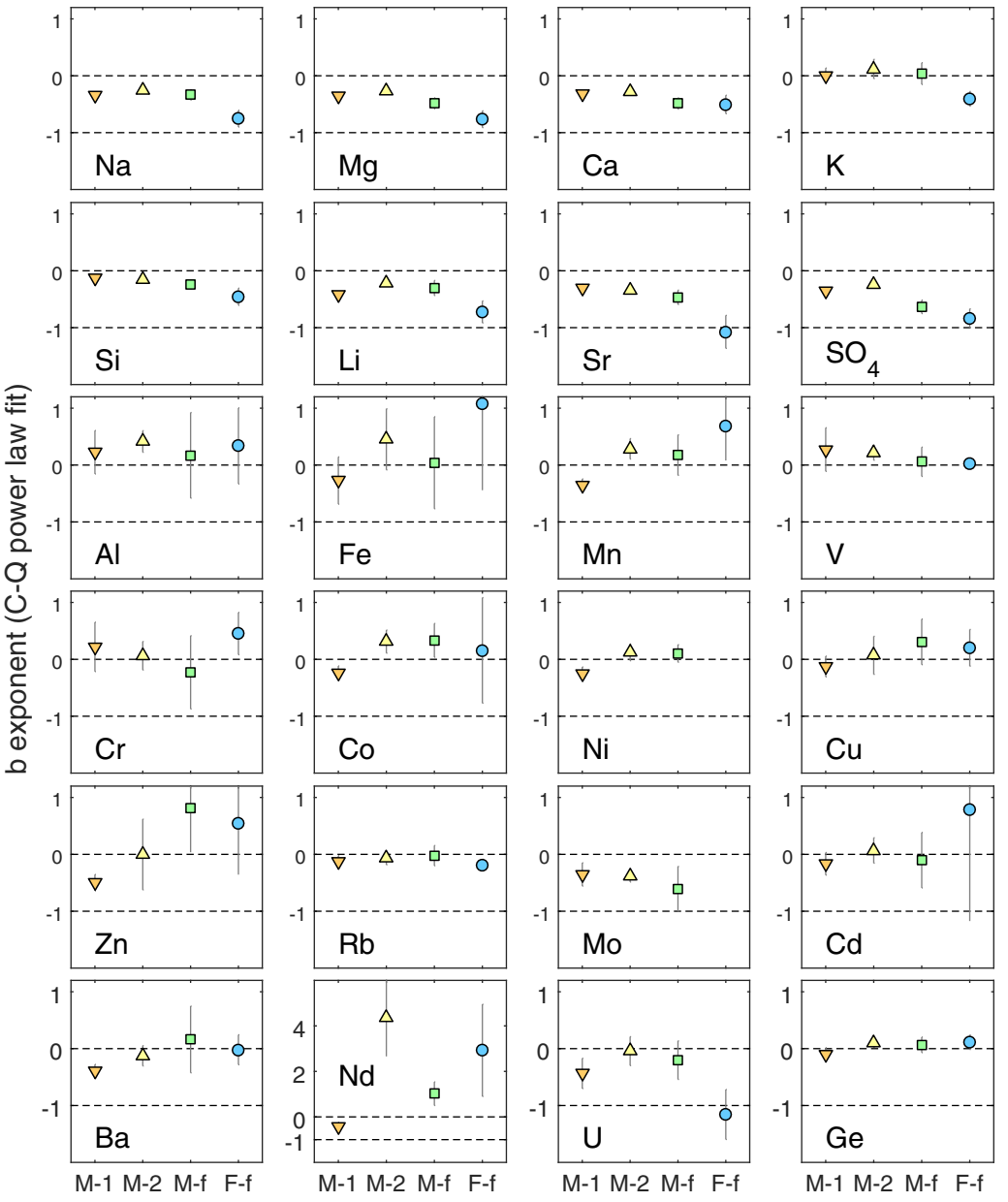

Figure 4. Slopes (*b* exponents) of concentration-runoff power law fits at the four nested catchment sites. M-1 = Mountain-1; M-2 = Mountain-2; M-f = Mountain-front; F-f = Foreland-floodplain. The horizontal dashed lines encompass *b* exponent values expected for dilutional-chemostatic behavior ($-1 < b < 0$). Error bars represent the 95% confidence interval (2σ in Table 3) and in some cases extend outside the plot bounds. Ni and Mo at Foreland-floodplain are not fit due to the small number of data points. Note the different *y* axis scale for Nd.

to the sampling site. Both tributaries have concentrations (C) that vary as a power law of runoff (Q) (equation (1)). Let us then imagine that they have different values of the preexponential parameter *a* but identical values of exponent *b*. If the mixing ratio of these tributaries varies with runoff (e.g., tributary 1 consistently contributes more solutes at high Q), then the resulting mixture will have a different *b* exponent value, despite the fact that the two mixing tributaries had the same value of *b*. In fact, the concentration of the sampled mixture does not have to be a power law function of discharge at all. This is also the case if the two tributaries have the same parameters *a* but different *b* exponents. In summary, C-Q relationships can be impacted by mixing if (1) C-Q relationships vary between contributing tributaries and (2) if the mixing ratio of these tributaries varies temporally. Below, we use our trace element data set to investigate the role of mixing in modulating C-Q relationships by identifying spatial variations in C-Q relationships and temporal variations in mixing ratios. We first consider how the C-Q dynamics of the Foreland-floodplain site are

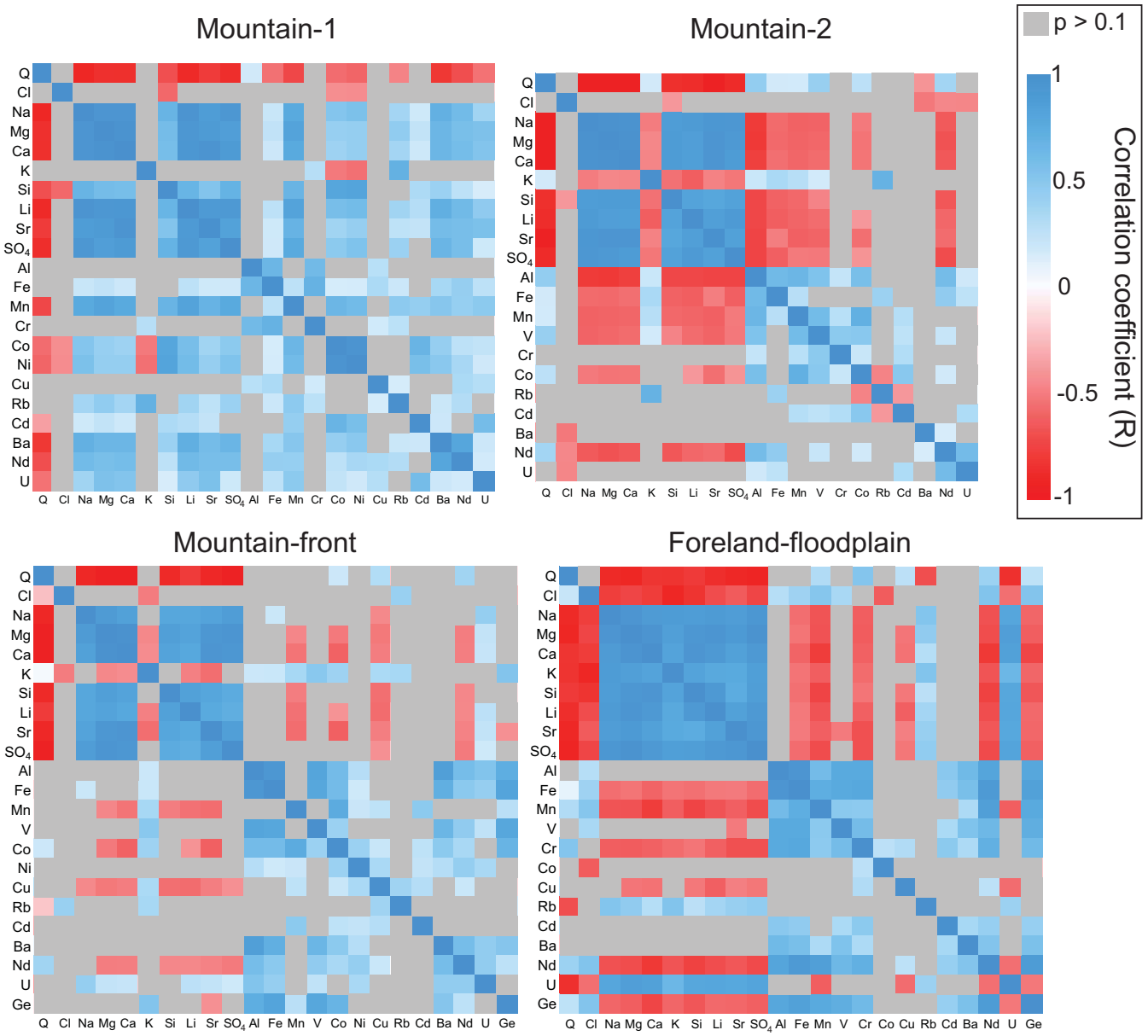

Figure 5. Correlation coefficients between major and trace element concentrations and runoff (Q). C-C correlations are calculated in linear space, whereas C-Q correlations are calculated after log-log transformation. Coefficients for correlations with $p > 0.1$ are grayed out. Note that the R and *p*-values calculated here are slightly different from those reported in Table 3 because only those samples that had all the represented solutes measured were used in the analysis here. The exact R and *p*-values are given for all significant and insignificant relationships in supporting information Table S3.

influenced by mixing of its major tributaries (section 4.1), and then how mixing affects the smaller Andean headwater catchments (section 4.2). Next, we evaluate the physical and chemical processes that may lead to heterogeneous solute production and associated mixing effects (section 4.3). Finally, we consider the implications of these results (section 4.4).

4.1. The Influence of Mixing on Concentration-Runoff Relationships at the Foreland-Floodplain Site

The Madre de Dios (MdD) catchment upstream of the Foreland-floodplain site can be divided into four main tributaries (Figure 1), of which the Alto Madre de Dios (represented by the Mountain-front site) and the Manu have the largest catchment areas and the majority of their catchment area within the Andes Mountains, which we define as greater than 400 m elevation (see companion paper by *Torres et al.* [2017]). In contrast, the Colorado and Chiribi Rivers have smaller catchment areas and a majority of their catchment areas is at less than 400 m elevation.

Table 4. Truly Dissolved and Colloidal Trace Element Concentrations in the Madre de Dios Catchment[a]

River	Concentration	Si (μmol/L)	Mn (μmol/L)	Fe (μmol/L)	Rb (nmol/L)	Ba (nmol/L)	Nd (nmol/L)	U (nmol/L)	V (nmol/L)	Co (nmol/L)
Alipachanca	Truly dissolved (<0.02 μm)	256.6	25.22	54.84	14.10	39.7	2.12	0.012	BDL	205
	Colloidal (0.02–0.2 μm)	BDL	BDL	BDL	BDL	0.6 ± 0.3	2.45 ± 0.06	0.032 ± 0.002	BDL	6.1 ± 5.8
	Colloidal fraction (%)	0 ± 3	0 ± 3	0 ± 3	0 ± 2	1 ± 1	54 ± 1	73 ± 5	n/a	3 ± 3
Huallpayuncha	Truly dissolved (<0.02 μm)	270.9	8.40	0.01	6.79	21.0	0.06	0.663	0.29	109
	Colloidal (0.02–0.2 μm)	0.9 ± 8.4	0.07 ± 0.22	0.1 ± 0	0.58 ± 0.15	4.6 ± 0.2	0.88 ± 0.01	0.152 ± 0.041	0.03 ± 0.01	4.43 ± 3.14
	Colloidal fraction (%)	0 ± 3	1 ± 3	89 ± 3	8 ± 2	18 ± 1	94 ± 1	19 ± 5	8 ± 2	4 ± 3
Mountain-1 (Kosñipata)	Truly dissolved (<0.02 μm)	194.9	6.61	4.29	5.47	23.9	0.38	0.110	BDL	136
	Colloidal (0.02–0.2 μm)	BDL	0.1 ± 0.18	0.58 ± 0.14	BDL	1.8 ± 0.2	1 ± 0.02	0.161 ± 0.013	BDL	1.1 ± 3.8
	Colloidal fraction (%)	0 ± 3	2 ± 3	12 ± 3	0 ± 2	7 ± 1	73 ± 1	59 ± 5	n/a	1 ± 3
Mountain-2 (Kosñipata)	Truly dissolved (<0.02 μm)	155.1	1.82	0.06	17.74	39.9	0.12	BDL	2.81	22.5
	Colloidal (0.02–0.2 μm)	3.44 4.9	0.05 ± 0.03	0.44 ± 0.01	0 ± 0.49	0.3 ± 2.2	0.96 ± 0.01	0.293 ± 0.031	0.19 ± 0.18	1.07 ± 1.98
	Colloidal fraction (%)	2 ± 3	3 ± 1	88 ± 3	0 ± 3	1 ± 6	89 ± 1	100 ± 11	6 ± 6	5 ± 8
Mountain-front (Alto MdD)	Truly dissolved (<0.02 μm)	194.1	0.60	0.03	13.20	47.9	0.13	0.027	6.07	3.17
	Colloidal (0.02–0.2 μm)	BDL	0.02 ± 0.02	0.11 ± 0	0.13 ± 0.26	BDL	0.12 ± 0	0.052 ± 0.004	BDL	BDL
	Colloidal fraction (%)	0 ± 3	3 ± 3	77 ± 3	1 ± 2	0 ± 1	48 ± 1	66 ± 5	0 ± 2	0 ± 3
Foreland-floodplain (Madre de Dios) 2016-05-25	Truly dissolved (<0.02 μm)	271.7	0.01	0.02	8.88	192.6	0.05	0.839	16.39	0.29
	Colloidal (0.02–0.2 μm)	BDL	0.12 ± 0	0.12 ± 0	0.11 ± 0.18	29.4 ± 1.6	0.6 ± 0.01	BDL	BDL	0.8 ± 0.03
	Colloidal fraction (%)	0 ± 3	96 ± 3	84 ± 3	1 ± 2	13 ± 1	93 ± 1	0 ± 5	0 ± 2	73 ± 3
Foreland-floodplain (Madre de Dios) 2016-05-28	Truly dissolved (<0.02 μm)	194.9	0.02	0.04	9.41	218.5	0.03	0.838	16.05	0.29
	Colloidal (0.02–0.2 μm)	BDL	0.08 ± 0	0.31 ± 0.01	BDL	50.7 ± 2	0.46 ± 0.01	BDL	0.32 ± 0.37	0.65 ± 0.03
	Colloidal fraction (%)	0 ± 3	84 ± 3	89 ± 3	0 ± 2	19 ± 1	94 ± 1	0 ± 5	2 ± 2	69 ± 3

[a]Alto Madre de Dios River samples are from the Mountain-front (MLC) site. BDL = below detection limit.

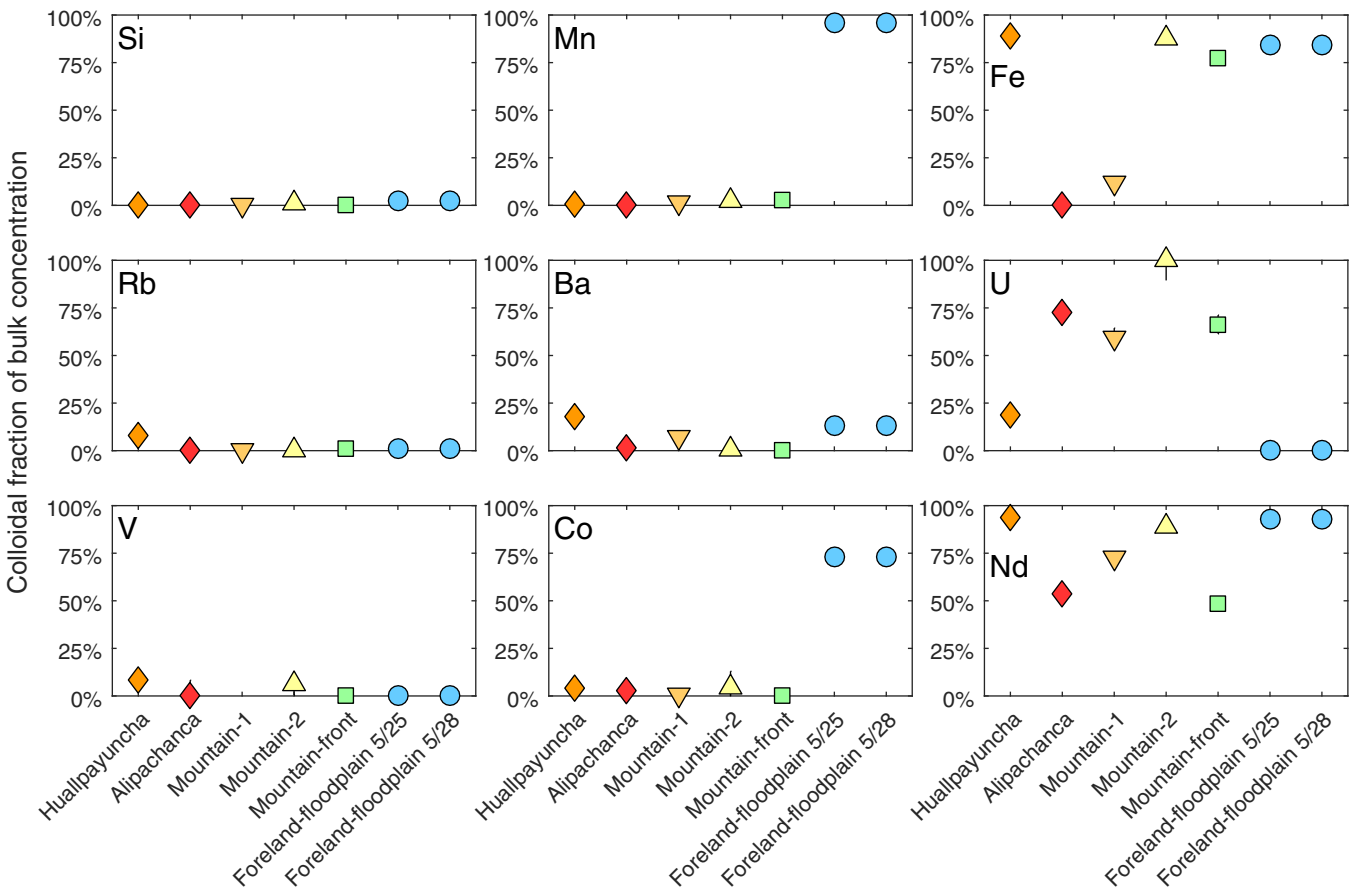

Figure 6. The colloidal (0.02–0.2 μm) fraction of several elements at the four nested catchments, as well as two Andean tributaries to the Kosñipata River immediately upstream of the Mountain-1 site (Figure 1). Samples were collected in May 2016. Vanadium concentrations at Mountain-1 were below detection limit. Errors were propagated from the analytical uncertainty on soluble (0.02 μm filtrate) and bulk dissolved (0.2 μm filtrate) concentrations and are in most cases smaller than the symbols.

Here we combine the water fluxes partitioned by tributary using the mixing model (see section 2 and *Torres et al*. [2017]) with the measured solute concentrations (supporting information Table S1) to apportion the contribution of each tributary to the total flux of each element at the Foreland-floodplain site (Figure 7). The tributaries represented in the mixing model comprise ~90% of the total MdD catchment area upstream of the Foreland-floodplain site. We note that these calculations assume conservative behavior for each individual solute, which is reevaluated in section 4.3.3. The results show that major elements, as well as Li, Sr, and U, are primarily supplied by the two tributaries with extensive Andean headwaters—the Alto Madre de Dios (Alto MdD) and the Manu. Importantly, the relative contribution of these elements by the Manu decreases significantly in the wet season due to an increase in the relative discharge of the other three tributaries (Figure 7) that are more dilute with regard to major ions, Li, Sr, and U (supporting information Table S1). As a result, the negative C-Q *b* exponents observed at the Foreland-floodplain site for these elements are to a large degree the result of decreasing contribution from the Manu. This is demonstrated in

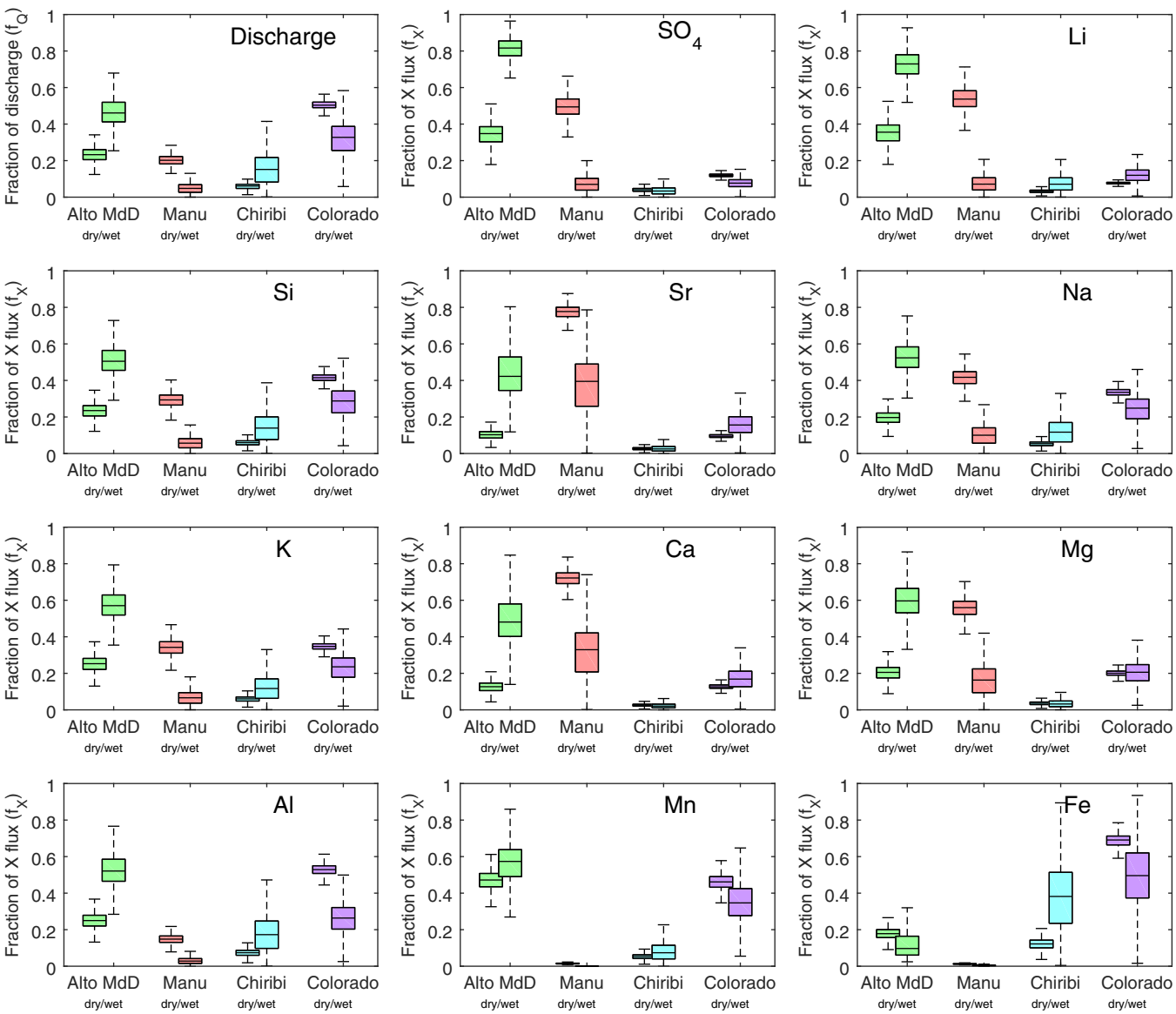

Figure 7. The fraction of the flux of water (f_Q) or a given element X (f_X) at the Foreland-floodplain site that is contributed by each of the four main tributaries during the dry and the wet seasons, as calculated using the tributary mixing model (see section 2.4.3 for details). The boxes reflect the interquartile range with the median shown as the line and the 1–99 percentiles as the whiskers. The median fractions sum up to 1 ± 0.03. The percentiles represent the full range of uncertainties and therefore not every f_X value within the uncertainty is compatible with every f_X value within the uncertainty for another tributary, due to the requirement to sum to 1. Note also that the calculated total flux of an element does not have to equal the flux measured at the Foreland-floodplain site (discussed in section 4.3.3). There were insufficient data available to do mixing model calculations for Ba, Mo, and Zn in the dry season.

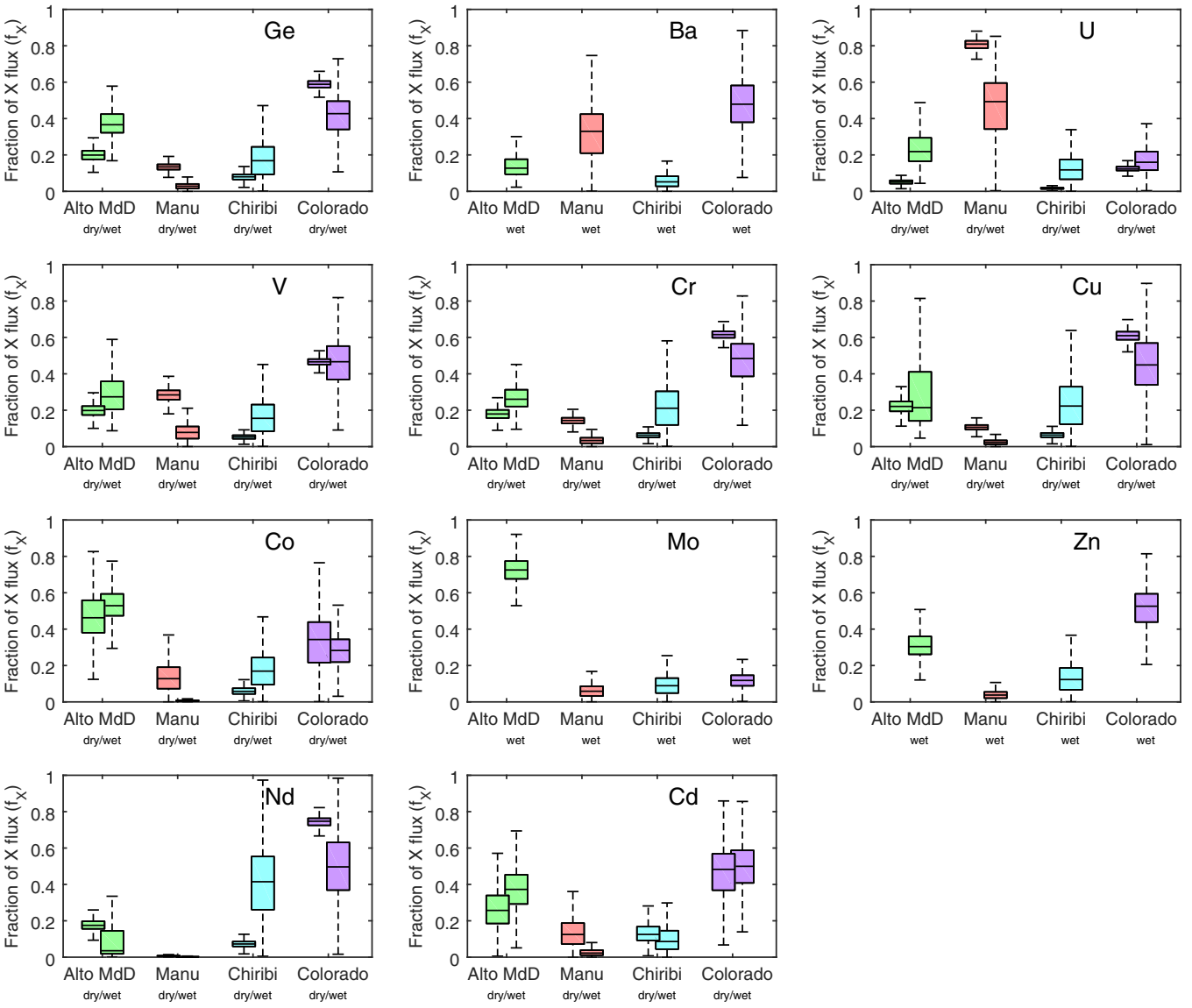

Figure 7. (continued).

Figure 8, which shows a clear correlation between the *b* exponent values of the C-Q relationships at the Foreland-floodplain site and the change in the relative flux of those elements from the Manu. Rb is likely to be a part of this group as well (see Figures 4 and 5); however, we lack data to include it in the tributary mixing model.

In contrast, the fluxes of most other trace metals are dominated by the Alto MdD and the Colorado (one of the lowland tributaries), with less input from the Manu. Despite often contrasting trace metal concentrations in the Alto MdD and the Colorado (supporting information Table S1), the fraction of flux contributed by each tributary, i.e., the effective mixing ratio, does not change significantly from dry to wet season (Figures 7 and 8). As a result, most of these trace metals exhibit *b* exponents indistinguishable from 0 within uncertainty and/or statistical significance (Table 3, Figure 4), as their concentrations are buffered by the relatively constant contribution from the lowland tributaries, especially the Colorado (Figures 7 and 8).

It therefore appears that the larger differences between *b* exponents of different elements (Figure 4) and the stronger anticorrelation of major and trace elements (Figure 5) observed at the Foreland-floodplain site relative to the smaller headwater catchments may result from discharge-dependent variations in the relative flux contributions from each of the major tributaries. Although a number of trace element *b* exponent

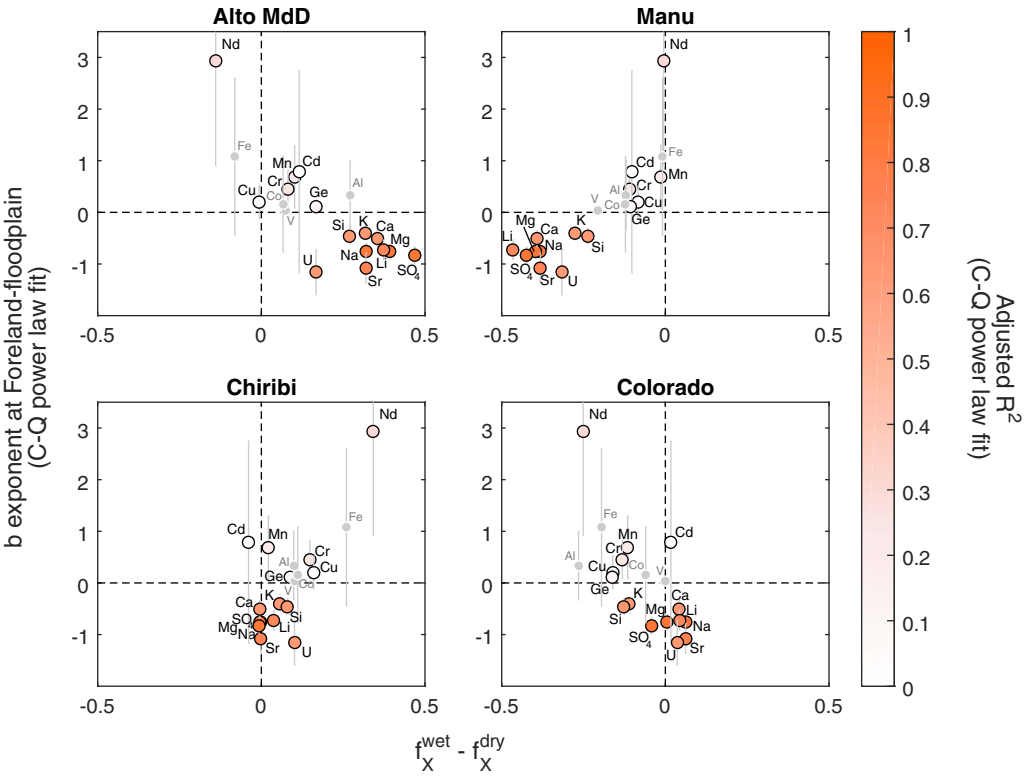

Figure 8. The slopes (*b* exponents) of C-Q power law fits in the Madre de Dios River at the Foreland-floodplain site (as shown in Figure 3) as a function of the seasonal (from dry to wet) change in the fraction of total flux of each element contributed by each of the four main tributaries (using median f_X values; see section 4.1 and Figure 7). Small gray symbols represent the elements for which the f_X-Q fit had a *p*-value above 0.1. The color of the larger symbols represents the degrees-of-freedom adjusted R^2 value of the C-Q power law fit. Error bars are the 95% confidence interval of the *b* exponent value.

values are derived from statistically weak C-Q fits (e.g., Al, Fe, V, and Co all have *p*-values > 0.1), they fit a relationship with the tributary mixing ratio (i.e., the *x* axis in the top two panels of Figure 8) that is consistent with the statistically significant ($p < 0.01$) *b* exponents (major elements, Li, Sr, Mn, Cr, Nd, U, and Ge).

The above discussion demonstrates the utility of analyzing and considering a large range of major and trace elements together. Tributary mixing effects would be much more difficult to detect if either the major or the trace elements were looked at in isolation (e.g., in Figure 8).

4.2. The Influence of Mixing on Concentration-Runoff Relationships in the Andes

Our results suggest that discharge-related variations in the relative contributions from different tributary subcatchments account for some of the variability in solute concentrations observed at the Foreland-floodplain site (~28,000 km^2 catchment area). Before analyzing the smaller catchments for analogous mixing effects, we note that with decreasing catchment elevation and increasing area most elements show systematic trends toward either more positive or more negative *b* exponents (Figure 4), and the major versus trace element anticorrelation becomes more apparent (Figure 5). Especially striking is the difference in *b* exponents between the two small Andean catchments. The smaller of the two—Mountain 1 (~50 km^2 area)—consistently exhibits *b* exponents between −0.5 and −0.2 for the vast majority of the analyzed elements (Table 3, Figure 4). In contrast, the trace element C-Q dynamics at Mountain-2, despite the catchment being only about three times larger (~160 km^2) than Mountain-1 and only about 10 km downstream (Figure 1), are much more akin (i.e., most trace element *b* exponents ~ 0) to those of the whole Alto MdD catchment (~6000 km^2) represented by the Mountain-front site (Figures 3 and 4). This suggests that the Mountain-2 catchment may include enough spatial heterogeneity to significantly affect some of the C-Q relationships observed at this site.

To further evaluate the aggregation effect on C-Q relationships at the Mountain-2 site, we have utilized a set of concentration-runoff sample pairs taken at the same time at the Mountain-2 and Mountain-1 sites, since

the latter comprises the upper portion of the catchment drained at Mountain-2 (Figure 1c). The upper (Mountain-1) and the lower (between Mountain-1 and Mountain-2) parts of the catchment exhibit contrasting C-Q relationships for a number of solutes (supporting information Figure S3) [see also *Torres et al*., 2017], indicating that there is potential for variable mixing to affect C-Q relationships observed at Mountain-2. To assess variability in tributary mixing for each of the elements in this study, we calculate the fraction of each solute flux (f_X, where X is the solute of interest) at Mountain-2 that is derived from its upper subcatchment Mountain-1, similar to the mixing model analysis of the Foreland-floodplain catchment presented above:

$$f_X = \frac{C_{Mountain-1} \times Q_{Mountain-1}}{C_{Mountain-2} \times Q_{Mountain-2}} \quad (3)$$

where C is the concentration of element X in mol/L and Q is the water discharge in L/d. The utilized samples and the calculated values are given in supporting information Table S4. This calculation assumes conservative behavior of solutes during mixing of tributaries within the Mountain-2 catchment, which may not always be valid, especially for trace elements during mixing of large tributaries (section 4.3.3). However, nonconservative behavior is likely to be less important in small catchments such as those discussed here.

The relationships between f_X and runoff at Mountain-2 for all the analyzed elements are shown in supporting information Figure S4. For all elements, the f_X values show either no relationship or decrease with increasing runoff at the Mountain-2 site, in the latter case indicating that the lower subcatchment, i.e., the area outside the Mountain-1 subcatchment (Figure 1c), contributes more solutes during periods of increased runoff. This mixing-runoff relationship is discussed in more detail in the companion paper [*Torres et al*., 2017]. The robustness of the f_X-Q trends can be tested through their respective R^2 and *p*-values (supporting information Figure S4). In the case of trace elements, due to the smaller number of concurrent data points available (n = 7–9), it is important to adjust the R^2 values for the number of the degrees-of-freedom in the fitting model, as this gives more robust (and usually lower) R^2 values (equation (2)). Lower *p*-values and higher adjusted R^2 values of the f_X-Q fit indicate a stronger relationship between the subcatchment mixing ratio and the observed runoff. Similarly to the Foreland-floodplain site, there appears to be a relationship between the element-specific *b* exponent and how strongly the flux of that element depends on a specific subcatchment at the Mountain-2 site—in other words, the extent to which the relative contributions from individual subcatchments vary with discharge—which can be represented by the adj. R^2 value (Figure 9) or the slope of the f_X-Q relationship (supporting information Figure S5).

For major and trace elements with *p*-values < 0.1, there is a clear relationship between either the adj. R^2 or the slope of f_X-Q fit and the *b* exponent of the C-Q fit, which suggests that runoff-related variations in tributary mixing contribute to differences in concentration-runoff relationships between different solutes. Solutes that have adj. R^2 values closer to zero are more evenly generated across the whole Mountain-2 catchment. This is the case for most major elements (Figure 9), which indicates that their lower *b* exponents are more likely to be the result of hillslope-scale processes rather than variable mixing. The controls on trace elements appear more complex, with generally positive *b* exponents regardless of the f_X-Q correlation, which may be the result of variable secondary reactions (see discussion below). The elements that are most affected by variable mixing (Al, Fe, Mn, Nd), however, tend to have the most positive *b* values, while K and Cd fall in-between (Figure 9). At high runoff, their concentrations at the Mountain-2 site increase, at the same time as the contribution from the Mountain-1 subcatchment decreases. As such, these solutes are mostly sourced from the lower part of the Mountain-2 catchment (i.e., the part that is not encompassed by the Mountain-1 subcatchment). The same conclusion is reached if the *b* exponent value is compared to the slope of the f_X-Q fit, although there are large uncertainties associated with both parameters (supporting information Figure S5). Overall, this analysis shows that the C-Q behavior of trace elements, and possibly some major elements, can be strongly influenced by spatial heterogeneity in catchments even as small as 160 km^2.

Even at the scale of the Mountain-1 catchment, there appears to be significant heterogeneity in solute generation. The Mountain-1 site is directly downstream of a confluence of two streams (Alipachanca and Huallpayuncha; Figure 1) that, based on one set of samples taken in May 2016, appear to have extremely different concentrations and size-partitioning of trace metals, such as Fe, Nd, U, and V. It is therefore peculiar that the C-Q relationships at this site do not exhibit similar range of *b* exponents as the larger catchments (Figure 4). However, variable tributary mixing does not necessarily have to result in a range of different C-Q behaviors, for example, if one of the tributaries consistently dominates the flux of all solutes. It

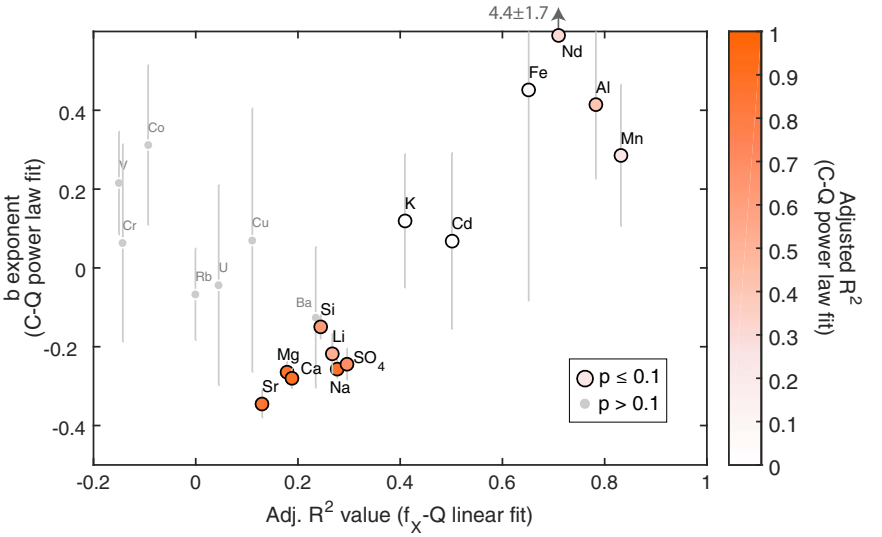

Figure 9. The slopes (*b* exponents) of C-Q power law fits for the Kosñipata River at the Mountain-2 site as a function of the degrees-of-freedom adjusted R^2 value for a linear fit between the fraction of solutes derived from the Mountain-1 subcatchment (f_X) and runoff (Q) at the Mountain-2 catchment. f_X was calculated using concentration-runoff measurements done at both sites at the same time (equation (3)). Small gray symbols represent the elements for which the f_X-Q fit had a *p*-value above 0.1. The color of the larger symbols represents the degrees-of-freedom adjusted R^2 value of the C-Q power law fit. Error bars are the 95% confidence interval of the *b* exponent value. Note that the set of analyzed trace elements is slightly different from Figure 8 due to the data available. f_X-Q relationship derived from n = 43 for major solutes and n = 7–9 for trace elements (see supporting information Figure S4).

is also possible that the relatively even rainfall distribution over the Mountain-1 catchment [*Clark et al.*, 2014] results in a relatively constant tributary mixing ratio even across a wide range of runoff values.

4.3. The Decoupling of Major and Trace Element C-Q Behavior

In the preceding discussion, we have demonstrated that the major and trace elements exhibit different C-Q relationships, both in the small Andean streams (section 4.2) as well as the larger Madre de Dios catchment (section 4.1). We ascribe this decoupling to variable mixing of tributaries with distinct C-Q relationships, especially in the case of trace metals. Concentrations of trace metals are known to be strongly impacted by secondary reactions, such as precipitation and adsorption on oxides and aluminosilicate clays [*Gaillardet et al.*, 2014, and references therein]. These reactions could potentially have a significant impact on the observed C-Q relationships, for example, if secondary mineral precipitation rates are sensitive to fluid flow paths and transit times, which are likely to change with runoff [*Godsey et al.*, 2009; *Maher*, 2011]. Full investigation of these effects, however, requires observations at the hillslope and soil profile level [for example, see *Kim et al.*, 2014, 2017] and is outside the scope of this study. Nonetheless, in this section, we provide an overview of the various aspects of the Madre de Dios system that can influence C-Q relationships by imposing differences on tributary chemistry, or through other means.

4.3.1. The Potential Role of Lithology and Anthropogenic Contamination

Compared to the monolithologic Mountain-1 catchment, a portion of the lower Kosñipata catchment drained at the Mountain-2 site is underlain by felsic plutonic igneous rocks (~20% of total catchment area) [*Clark et al.*, 2014], which may be the cause of distinct C-Q relationships of multiple solutes (especially trace elements) when comparing between the upper and the lower parts of the catchment (as described in section 4.2) [also see *Torres et al.*, 2017]. While the Kosñipata (Mountain-1 and Mountain-2) and Alto MdD (Mountain-front) catchments are primarily underlain by Paleozoic shales and a plutonic unit, the larger MdD catchment as sampled at the Foreland-floodplain site incorporates a much wider array of sedimentary deposits of various ages [*Torres et al.*, 2016]. Based on the high Mg and Ca concentrations (Table 2), the Manu tributary is likely to be draining a more carbonate-rich lithology. As a result, carbonate-supplied elements should have C-Q relationships with a much higher pre-exponential parameter a (equation (1)) in the Manu compared to the other tributaries, rendering them more sensitive to mixing effects at the Foreland-floodplain site. Besides Ca and Mg, this effect is also apparent for Sr and U (Figures 7 and 8), which are trace elements often mobilized from carbonate rock dissolution [e.g., *Gaillardet et al.*, 2014] and are indeed observed at high concentrations in the Manu river (supporting information Table S1).

The lowland tributaries (the Chiribi and the Colorado) primarily drain younger (Holocene to Paleogene) deposits, which may explain their distinct concentrations and C-Q responses of many elements (supporting information Table S1) relative to the Andean tributaries. Additionally, there is significant gold mining activity on the banks of the lower Madre de Dios River and especially within the Colorado subcatchment [*Asner et al*., 2013], and these activities may have an effect on the dissolved concentrations of some trace elements.

4.3.2. The Potential Role of Heterogeneous Geomorphology

Increasing catchment area across our study sites results not only in a more complex lithology but also in a much larger drained elevation range (Table 1). The elevation gradient in the eastern Andes is strongly associated with gradients in precipitation [*Espinoza et al*., 2009; *Clark et al*., 2014] and erosion rates [*Safran et al*., 2005]. Precipitation and erosion are both thought to exert strong controls on solute generation via chemical weathering [*West*, 2012; *Maher and Chamberlain*, 2014], so the increasing heterogeneity in these parameters could also explain the increasingly stronger mixing effects downstream.

Previous work has shown that the rainfall distribution is fairly uniform in the Mountain-1 catchment, whereas the Mountain-2 catchment spans a larger range of elevations and therefore a large precipitation gradient [*Clark et al*., 2014]. During the wet season, a large proportion of the runoff is generated in a relatively narrow elevation range within the lower part of the catchment (outside of what is the Mountain-1 subcatchment), whereas during the dry season the precipitation distribution is more even, allowing for a larger contribution from Mountain-1. The precipitation distribution is even more heterogeneous in the Alto MdD (sampled at Mountain-front) and in the full MdD (sampled at Foreland-floodplain) catchments, potentially causing the larger variability of element C-Q relationships observed at these sites (Figure 4). A companion paper [*Torres et al*., 2017] shows that the seasonal variations in tributary mixing proportions at the Foreland-floodplain site are consistent with the spatiotemporal rainfall patterns across the MdD catchment [*Torres et al*., 2017, Figures 6 and 8].

Additionally, the highly dampened amplitude of seasonal water isotope variations at the Andes Mountains sites suggests significant water storage in deep fractures within the shale and granite bedrock of the Kosñipata catchment [*Clark et al*., 2014]. A less dampened amplitude of water isotope variations in the Foreland-floodplain [*Ponton et al*., 2014] suggests that fluid flow paths may be shallower and transit times shorter in the lowland catchments, which could manifest as differences in the chemistry of Andean versus lowland tributaries [*Torres et al*., 2015].

Spatial heterogeneity in a number of other catchment properties, such as hillslope steepness, vegetation cover, erosion, and landslide rates, to name a few, also scale with catchment area and may impact C-Q dynamics at our study sites. For example, *Clark et al*. [2016] showed that the lower portion of the Kosñipata catchment has a higher landslide occurrence rate compared to the upper part, likely due to steeper slope angles and more frequent intense precipitation events. Landslide events have been shown to impact chemical weathering rates [*Emberson et al*., 2015] and therefore may contribute to spatiotemporal variability in riverine solute concentrations.

4.3.3. The Potential Role of Colloid Dynamics and Nonconservative Behavior

The association of certain trace elements with colloidal particles may also play an important role in C-Q dynamics, especially in the Foreland-floodplain, where lowland tributaries are likely to supply abundant organic compounds [e.g., *Stallard and Edmond*, 1983; *Benedetti et al*., 2003]. While changes in element size-partitioning between soluble and colloidal phases would not affect the bulk concentrations investigated here, colloidal particles may help remove elements from solution if they were to aggregate [e.g., *Benedetti et al*., 2003; *Aucour et al*., 2003; *Bouchez et al*., 2011; *Mulholland et al*., 2014] to form particles large enough to be caught in our filters (>0.2 μm). However, in our data set, there does not appear to be a consistent pattern in trace element size-partitioning along the geomorphic gradient that could explain the near-universal change in trace element C-Q dynamics from Mountain-1 to Mountain-2 and further to the Foreland-floodplain. For example, Ba and V are only found in the soluble phase across all sites, whereas a significant fraction of Fe and Nd are found in the colloidal phase (Figure 6). Mn and Co become strongly associated with colloids only in the Foreland-floodplain, which may explain their overall lower concentrations at that site (Figure 2). Despite this variable size-partitioning, all these elements are generally correlated with each other across all four sites investigated (Figure 5) and display variable C-Q behavior that is uncorrelated with their size-partitioning (Figure 4). There is, however, the possibility that the size-partitioning of certain elements is also dependent on runoff and seasonality,

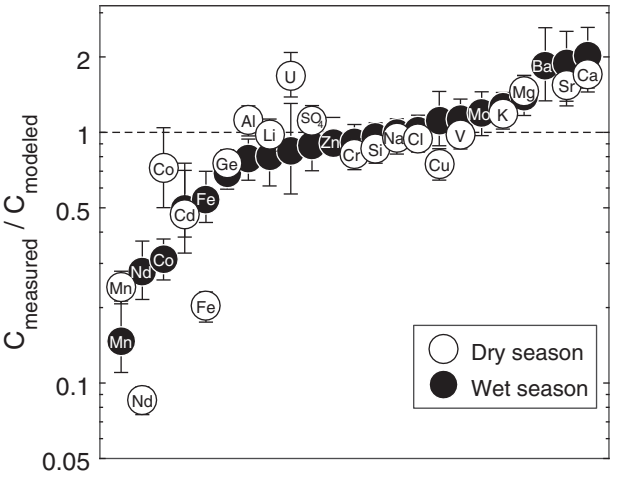

Figure 10. The degree of nonconservative behavior of major and trace elements at the Foreland-floodplain site, defined as the ratio between the measured concentrations and those predicted using the tributary mixing model (see section 4.3.3). Values <1 represent nonconservative loss of solute from solution, while values >1 represent addition.

and the snapshot provided by this sample set does not reflect such temporal dynamics. Future studies separating the soluble and the colloidal C-Q behavior are needed to assess such potential variability.

The importance of changes in the size distribution of different elements can also be explored by evaluating their behavior during mixing. The tributary mixing model allows us to compare the concentrations measured at the Foreland-floodplain site to those predicted if mixing of all tributaries were conservative for each investigated element (Figure 10). Since the mixing model is calibrated using Na and Cl (section 2.4.3), their behavior is by definition conservative. In the case of Si and SO_4, the modeled and measured concentrations agree within uncertainty. This result is unsurprising, as these solutes are generally considered conservative. Nevertheless, it helps to confirm the robustness of the mixing model and the calculated tributary mixing proportions (Figure 7). Many trace elements behave for the most part conservatively as well (Li, Al, Cu, Cr, V, Mo, Zn), whereas a few in particular (Mn, Nd, Fe, Co, Cd) are strongly affected by nonconservative reactions (Figure 10). It is therefore possible that the latter elements are lost from solution due to coagulation of colloids—indeed, Mn, Fe, Nd, and Co are all primarily colloidal (Table 4, Figure 6) and also are most strongly removed from solution at some point during tributary mixing between the Mountain-front and Foreland-floodplain sites (Figure 10). Alternatively, adsorption onto suspended load may play a role in their loss from solution. Whatever the cause, nonconservative behavior would have to systematically shift with runoff for it to affect the observed C-Q relationships.

A link between nonconservative behavior and runoff could result from runoff-dependent in-channel water residence time, or from changes in solution chemistry due to variable tributary mixing, which would affect the thermodynamic state of the solution and the kinetics of reactions between the suspended and dissolved load (e.g., dissolution of bed load material or precipitation of secondary minerals). Many primary and secondary mineral saturation indices may vary with runoff, but this variability is difficult to assess without robust pH constraints (see section 2.4.4). Nevertheless, it does appear that several primary minerals, e.g., K-feldspar and albite, are likely to be relatively close to equilibrium or even potentially supersaturated (SI = ~–2 to 1), and various shale-sourced and secondary clays are consistently supersaturated (SI = ~2–15), across all sites and regardless of runoff (supporting information Table S5). The near-equilibrium chemistry may help buffer the concentrations of some solutes, e.g., resulting in the relatively chemostatic K and Si behavior (Figure 4), though more robust thermodynamic calculations would help test this hypothesis. On the other hand, calcite and dolomite remain undersaturated (SI = ~–3 to −2, in most cases), suggesting a smaller buffering capacity, which is consistent with the lower *b* exponents for carbonate-associated elements such as Ca, Mg, and Sr. Carbonate undersaturation also helps explain the mixing model results showing the nonconservative addition of dissolved Ca, Mg, Sr, and Ba during fluid transit across the floodplain in both seasons (Figure 10), most likely due to continued carbonate dissolution in or nearby the river channel (i.e., in the riparian and hyporheic zones). This observation supports previous indications of continued carbonate dissolution during transport, based on suspended load chemistry in the lower reaches of this river system [*Bouchez et al*., 2012].

In the case of trace elements such as Al, Fe, Mn, Nd, Cr, and Co, nonconservative removal would have to be stronger in the dry season to cause positive C-Q *b* exponents (Figure 4). Thermodynamic calculations indicate that a large number of secondary oxides and clays are supersaturated in the river water (supporting information Table S5). The supersaturation of many phyllosilicates, such as kaolinite and smectite, appears to be higher during low runoff, while the reverse is true for Al and Fe oxides, such as gibbsite and $Fe(OH)_3$.

Whether these changes are sufficient to explain C-Q dynamics remains to be determined, since we do not know the detailed association of specific trace elements with different secondary phases. However, there does not appear to be a consistent seasonal trend in the nonconservative loss of trace elements from solution (Figure 10).

Other factors that are outside the scope of this study, such as the rates of secondary phase precipitation reactions, the concentration and composition of dissolved organic matter, and mineral surface adsorption dynamics are all likely to vary in some way with runoff and to influence the observed trace element C-Q relationships. Finally, the mixing model used here, based on sampling at two time-points, is unlikely to be capturing the full dynamics of nonconservative behavior. Altogether, the potential for physical and chemical processes within or near the river channel to alter solute concentrations is poorly constrained but our analysis demonstrates that it could potentially act in concert with changes in water sources (see sections 4.3.1 and 4.3.2) to impact both major and trace element C-Q dynamics (Figure 10). This conclusion is in agreement with data recently obtained from a small catchment in Santa Catalina Mountains in Arizona, USA, where colloidal dynamics have been shown to strongly influence the observed trace element C-Q relationships [*Trostle et al*., 2016]. Colloidal and in-channel processes deserve more careful investigation in the future.

4.4. Implications for the Interpretation of C-Q Relationships

Our data indicate that changes in tributary mixing proportions contribute significantly to determining the C-Q relationships of some elements across the sites in this study. These results suggest that other studies investigating temporal variation of solute chemistry should carefully consider the potential role of mixing and tributary aggregation effects, including at the scale of catchments $\sim$100 km^2 in area. Many of the catchments studied in detail in past work have been of this size [e.g., *Tipper et al*., 2006; *Godsey et al*., 2009; *Calmels et al*., 2011; *Ibarra et al*., 2016]. Isolating the effects of hillslope-scale processes, such as variations in mineral and fluid residence times [cf., *Torres et al*., 2015], therefore will require either explicitly addressing tributary mixing effects or focusing attention on even smaller, more homogeneous catchments.

In addition, elemental ratio-runoff or isotopic ratio-runoff relationships could similarly be influenced by aggregation. In the case of very large river systems, the effect from mixing of tributaries with distinct isotopic composition has been readily acknowledged when interpreting dynamics of solute isotope ratios [e.g., *Cardinal et al*., 2010; *Tipper et al*., 2012; *Voss et al*., 2014; *Henchiri et al*., 2016]. However, many studies of smaller systems have interpreted elemental-runoff or isotope ratio-runoff relationships as reflecting changes in weathering style and cation sources (e.g., carbonate versus silicate), attributed to either changing fluid flow paths in idealized hillslopes [e.g., *Galy and France-Lanord*, 1999; *Calmels et al*., 2011; *Mavromatis et al*., 2014; *Torres et al*., 2015] or thermodynamically induced changes in mineral reaction rates [e.g., *Georg et al*., 2006; *Tipper et al*., 2006; *Moon et al*., 2007]. Our study suggests that to allow such interpretations, the spatial homogeneity of a catchment has to be established, i.e., all the tributaries should have similar ratios and should have similar ratio-runoff relationships. If they do not, then it has to be established that the ratio-runoff relationship at the sampled site is not due to variable tributary mixing upstream before the change of elemental or isotopic ratio can be robustly interpreted as a weathering reaction response to hydrology.

Conversely, the isotopic composition of solutes and their variations with runoff can provide additional evidence of mixing processes (or lack thereof). For example, the companion paper [*Torres et al*., 2017] shows how the isotopic composition of sulfate can be used to confirm that mixing is the first-order driver of observed sulfate chemistry variations with runoff at the Foreland-floodplain site. Therefore, in cases where tributaries have distinct solute isotope compositions (e.g., due to lithologic differences), they can be used to track solute generation in different parts of a catchment and how it varies with time or hydrological regime.

5. Conclusions

We have investigated the concentration-runoff (C-Q) dynamics of a suite of major and trace elements in nested catchments spanning the gradient from the Andes Mountains to the Amazon Foreland-floodplain. Compared to major solutes, trace element concentrations vary more and over shorter time scales. Whereas most major solutes display some degree of dilution with increasing runoff (negative power law *b*

exponents), most trace elements either show no relationship with runoff or exhibit higher concentrations at high runoff (positive power law *b* exponents). The differences between major and trace element behavior become stronger with increasing catchment area and elevation range.

The observed concentration-runoff relationships appear to be strongly influenced by variations in tributary mixing that are correlated with runoff, potentially explaining the decoupling in major and trace element behavior. As catchment area and drained elevation ranges increase, so does the spatiotemporal variability in precipitation, resulting in more systematic variations in tributary mixing ratios. Because different tributaries exhibit different concentration ranges and C-Q patterns of some elements, a change in their mixing proportions has an effect on the C-Q relationship observed downstream. The variable tributary C-Q relationships could be the result of spatial variability in geomorphology, lithology, or precipitation, or any combination thereof. Tributary mixing affects both major and trace elements to variable degrees and is observed across the range of nested catchments.

Additional controls on trace element concentrations may be imposed by the association of some elements with colloidal particles, as well as nonconservative behavior (removal from or addition to solution) during transport—for example, during mixing of tributaries with distinct solid or dissolved chemical compositions. Further research is needed, however, to assess how changes in runoff may affect these processes and to constrain their effect on concentration-runoff dynamics.

Overall, our results suggest that in the Kosñipata and Madre de Dios watersheds, and potentially other watersheds of similar size (>160 km^2) and perhaps even smaller, concentration-runoff relationships are governed not solely by the weathering reactions and the intrinsic properties of the critical zone but also by heterogeneity of solute generation and runoff generation within catchments. While this may not be the case for all catchments, inferences about hillslope-scale solute generation models and trace element behavior under changing hydrological conditions should carefully consider the potentially confounding effects of mixing as observed here. Multiple trace elements appear especially sensitive to spatial heterogeneity in catchment lithology and/or geomorphology in our studied system.

Acknowledgments
All the geochemical data used are listed in the tables and in supporting information Table S2. The water discharge data have been published in association with cited studies [*Clark et al*., 2014; *Torres et al*., 2015] and are included for reference in supporting information Table S2. The MATLAB code for the tributary mixing model (including all the trace elements) is attached in the supporting information. We thank ACCA Peru (Wayqecha and CICRA), Manu Learning Centre (MLC), and Incaterra (San Pedro) for field support, and A. Robles Caceres, L. V. Morales, D. Lima Llasa, E. Nunoncca Sencia, R. J. Abarca Martnez, M. H. Yucra Hurtado, R. Paja Yurca, J. A. Gibaja Lopez, I. Cuba Torres, J. Huamn Ovalle, A. Alfaro-Tapia, R. Butrn Loayza, J. Farfan Flores, D. Oviedo Licona, D. Ocampo, Y. Gutierrez Usca, J. F. Costa Taborga, C. Jones, and S. Federman for field assistance collecting the 2010–2011 samples. Sample collection and processing was done with the help of Sarah Feakins, Camilo Ponton, Valier Galy, and Adan Ccahuana in 2013, and Emily Burt and the USC Field Geology class in 2016, with assistance from ACCA Peru. This research was supported by grants NSF-EAR 1455352 and NSF EAR-1227192 to A. J. West. K. Clark was supported by the Natural Sciences and Engineering Research Council of Canada (NSERC) and Clarendon Fund PhD scholarships. M. Torres was supported by USC College Doctoral and Center for Dark Energy Biosphere Investigations (C-DEBI) fellowships. We thank Jean-Sébastien Moquet, Julien Bouchez, and an anonymous reviewer for thoughtful and constructive comments. Gen Li is thanked for helpful discussions prior to submission. This is a contribution to the Andes Biodiversity and Ecosystems Research Group.

References

Admiraal, D., and M. Demissie (1996), Velocity and discharge measurements at selected locations on the Mississippi river during the Great Flood of 1993 using an Acoustic Doppler Current Profiler, *Water Int.*, *21*(3), 144–151.

Ameli, A. A., K. Beven, M. Erlandsson, I. F. Creed, J. J. McDonnell, and K. Bishop (2017), Primary weathering rates, water transit times, and concentration-discharge relations: A theoretical analysis for the critical zone, *Water Resour. Res.*, *53*, 942–960, doi:10.1002/2016WR019448.

Archer, C., and D. Vance (2008), The isotopic signature of the global riverine molybdenum flux and anoxia in the ancient oceans, *Nat. Geosci.*, *1*(9), 597–600, doi:10.1038/ngeo282.

Asner, G. P., W. Llactayo, R. Tupayachi, and E. R. Luna (2013), Elevated rates of gold mining in the Amazon revealed through high-resolution monitoring, *Proc. Natl. Acad. Sci. U. S. A.*, *110*(46), 18,454–18,459, doi:10.1073/pnas.1318271110.

Aucour, A.-M., F.-X. Tao, P. Moreira-Turcq, P. Seyler, S. Sheppard, and M. Benedetti (2003), The Amazon River: Behaviour of metals (Fe, Al, Mn) and dissolved organic matter in the initial mixing at the Rio Negro/Solimes confluence, *Chem. Geol.*, *197*(1–4), 271–285, doi:10.1016/S0009-2541(02)00398-4.

Bagard, M. L., F. Chabaux, O. S. Pokrovsky, J. Viers, A. S. Prokushkin, P. Stille, S. Rihs, A. D. Schmitt, and B. Dupré (2011), Seasonal variability of element fluxes in two Central Siberian rivers draining high latitude permafrost dominated areas, *Geochim. Cosmochim. Acta*, *75*(12), 3335–3357, doi:10.1016/j.gca.2011.03.024.

Baronas, J. J., D. E. Hammond, W. M. Berelson, J. McManus, and S. Severmann (2016), Germanium-silicon fractionation in a river-influenced continental margin: The Northern Gulf of Mexico, *Geochim. Cosmochim. Acta*, *178*, 124–142, doi:10.1016/j.gca.2016.01.028.

Benedetti, M. F., S. Mounier, N. Filizola, J. Benaim, and P. Seyler (2003), Carbon and metal concentrations, size distributions and fluxes in major rivers of the Amazon basin, *Hydrol. Processes*, *17*(7), 1363–1377, doi:10.1002/hyp.1289.

Bern, C. R., O. A. Chadwick, A. S. Hartshorn, L. M. Khomo, and J. Chorover (2011), A mass-balance model to separate and quantify colloidal and solute redistributions in soil, *Chem. Geol.*, *282*(3–4), 113–119, doi:10.1016/j.chemgeo.2011.01.014.

Berner, R., A. Lasaga, and R. Garrels (1983), The carbonate-silicate geochemical cycle and its effect on atmospheric carbon dioxide over the past 100 million years, *Am. J. Sci.*, *283*, 641–683.

Berner, R. A. (1992), Weathering, plants, and the long-term carbon cycle, *Geochim. Cosmochim. Acta*, *56*(8), 3225–3231, doi:10.1016/0016-7037(92)90300-8.

Berner, R. A., and J. L. Rao (1994), Phosphorus in sediments of the Amazon River and estuary: Implications for the global flux of phosphorus to the sea, *Geochim. Cosmochim. Acta*, *58*(10), 2333–2339, doi:10.1016/0016-7037(94)90014-0.

Bouchez, J., F. Métivier, M. Lupker, L. Maurice, M. Perez, J. Gaillardet, and C. France-Lanord (2011), Prediction of depth-integrated fluxes of suspended sediment in the Amazon River: Particle aggregation as a complicating factor, *Hydrol. Processes*, *25*(5), 778–794, doi:10.1002/hyp.7868.

Bouchez, J., J. Gaillardet, M. Lupker, P. Louvat, C. France-Lanord, L. Maurice, E. Armijos, and J.-S. Moquet (2012), Floodplains of large rivers: Weathering reactors or simple silos?, *Chem. Geol.*, *332–333*, 166–184, doi:10.1016/j.chemgeo.2012.09.032.

Boyer, E. W., R. W. Howarth, J. N. Galloway, F. J. Dentener, P. A. Green, and C. J. Vörösmarty (2006), Riverine nitrogen export from the continents to the coasts, *Global Biogeochem. Cycles*, *20*, GB1S91, doi:10.1029/2005GB002537.

Brezonik, P. L., C. E. Mach, and C. J. Sampson (2003), Geochemical controls for Al, Fe, Mn, Cd, Cu, Pb, and Zn during experimental acidification and recovery of Little Rock Lake, WI, USA, *Biogeochemistry*, *62*(2), 119–143, doi:10.1023/A:1021167917839.

Bruland, K. W., R. Middag, and M. C. Lohan (2013), Controls of trace metals in seawater, in *Treatise on Geochemistry: Second Edition*, vol. 8, 2nd ed., pp. 19–51, Elsevier, Hoboken, N. J., doi:10.1016/B978-0-08-095975-7.00602-1.

Calmels, D., A. Galy, N. Hovius, M. Bickle, A. J. West, M.-C. Chen, and H. Chapman (2011), Contribution of deep groundwater to the weathering budget in a rapidly eroding mountain belt, Taiwan, *Earth Planet. Sci. Lett.*, *303*(1–2), 48–58, doi:10.1016/j.epsl.2010.12.032.

Cardinal, D., J. Gaillardet, H. J. Hughes, S. Opfergelt, and L. André (2010), Contrasting silicon isotope signatures in rivers from the Congo Basin and the specific behaviour of organic-rich waters, *Geophys. Res. Lett.*, *37*, L12403, doi:10.1029/2010GL043413.

Carlotto Caillaux, V. S., G. Rodriguez, W. Fernando, C. Roque, J. Dionicio, and R. Chávez (1996), Geología de los cuadrángulos de Urubamba y Calca, technical report 27-rs, Inst. Geol. Nac., Lima.

Cerling, T. E., and R. R. Turner (1982), Formation of freshwater Fe-Mn coatings on gravel and the behavior of ^{60}Co, ^{90}Sr, and ^{137}Cs in a small watershed, *Geochim. Cosmochim. Acta*, *46*(8), 1333–1343, doi:10.1016/0016-7037(82)90269-1.

Clark, K. E., R. G. Hilton, A. J. West, Y. Malhi, D. R. Gröcke, C. L. Bryant, P. L. Ascough, A. Robles Caceres, and M. New (2013), New views on old carbon in the Amazon River: Insight from the source of organic carbon eroded from the Peruvian Andes, *Geochem. Geophys. Geosyst.*, *14*, 1644–1659, doi:10.1002/ggge.20122.

Clark, K. E., M. A. Torres, A. J. West, R. G. Hilton, M. New, A. B. Horwath, J. B. Fisher, J. M. Rapp, A. Robles Caceres, and Y. Malhi (2014), The hydrological regime of a forested tropical Andean catchment, *Hydrol. Earth Syst. Sci.*, *18*(12), 5377–5397, doi:10.5194/hess-18-5377-2014.

Clark, K. E., et al. (2016), Storm-triggered landslides in the Peruvian Andes and implications for topography, carbon cycles, and biodiversity, *Earth Surf. Dyn.*, *4*(1), 47–70, doi:10.5194/esurf-4-47-2016.

Clow, D. W., and M. A. Mast (2010), Mechanisms for chemostatic behavior in catchments: Implications for CO_2 consumption by mineral weathering, *Chem. Geol.*, *269*(1–2), 40–51, doi:10.1016/j.chemgeo.2009.09.014.

Creed, I. I. F., et al. (2015), The river as a chemostat: Fresh perspectives on dissolved organic matter flowing down the river continuum, *Can. J. Fish. Aquat. Sci.*, *14*, 1–14, doi:10.1139/cjfas-2014-0400.

Dellinger, M., J. Gaillardet, J. Bouchez, D. Calmels, P. Louvat, A. Dosseto, C. Gorge, L. Alanoca, and L. Maurice (2015), Riverine Li isotope fractionation in the Amazon River basin controlled by the weathering regimes, *Geochim. Cosmochim. Acta*, *164*, 71–93, doi:10.1016/j.gca.2015.04.042.

Derry, L., and C. France-Lanord (1996), Neogene Himalayan weathering history and river ^{87}Sr^{86}Sr: Impact on the marine Sr record, *Earth Planet. Sci. Lett.*, *142*, 59–74.

Derry, L. A., J. C. Pett-Ridge, A. C. Kurtz, and J. W. Troester (2006), Ge/Si and ^{87}Sr/^{86}Sr tracers of weathering reactions and hydrologic pathways in a tropical granitoid system, *J. Geochem. Explor.*, *88*(1–3), 271–274, doi:10.1016/j.gexplo.2005.08.054.

Dürr, H. H., M. Meybeck, J. Hartmann, G. G. Laruelle, and V. Roubeix (2011), Global spatial distribution of natural riverine silica inputs to the coastal zone, *Biogeosciences*, *8*(3), 597–620, doi:10.5194/bg-8-597-2011.

Durum, W. H. (1953), Relationship of the mineral constituents in solution to stream flow, Saline River near Russell, Kansas, *Trans. AGU*, *34*(3), 435–442, doi:10.1017/CBO9781107415324.004.

Emberson, R., N. Hovius, A. Galy, and O. Marc (2015), Chemical weathering in active mountain belts controlled by stochastic bedrock landsliding, *Nat. Geosci.*, *9*, 42–45, doi:10.1038/ngeo2600.

Erel, Y., J. J. Morgan, and C. C. Patterson (1991), Natural levels of lead and cadmium in a remote mountain stream, *Geochim. Cosmochim. Acta*, *55*(3), 707–719, doi:10.1016/0016-7037(91)90335-3.

Espinoza, J. C., J. Ronchail, J. L. Guyot, G. Cochonneau, F. Naziano, W. Lavado, E. De Oliveira, R. Pombosa, and P. Vauchel (2009), Spatio-temporal rainfall variability in the Amazon basin countries (Brazil, Peru, Bolivia, Colombia, and Ecuador), *Int. J. Climatol.*, *29*(11), 1574–1594, doi:10.1002/joc.1791.

Frings, P. J., W. Clymans, G. Fontorbe, C. L. De La Rocha, and D. J. Conley (2016), The continental Si cycle and its impact on the ocean Si isotope budget, *Chem. Geol.*, *425*, 12–36, doi:10.1016/j.chemgeo.2016.01.020.

Gaillardet, J., B. Dupré, P. Louvat, and C. Allègre (1999), Global silicate weathering and CO_2 consumption rates deduced from the chemistry of large rivers, *Chem. Geol.*, *159*(1–4), 3–30, doi:10.1016/S0009-2541(99)00031-5.

Gaillardet, J., J. Viers, and B. Dupré (2014), Trace elements in river waters, in *Treatise on Geochemistry*, 2nd ed., chap. 7.7, pp. 195–235, Elsevier, Hoboken, N. J., doi:10.1016/B978-0-08-095975-7.00507-6.

Galy, A., and C. France-Lanord (1999), Weathering processes in the Ganges-Brahmaputra basin and the riverine alkalinity budget, *Chem. Geol.*, *159*(1–4), 31–60, doi:10.1016/S0009-2541(99)00033-9.

Georg, R., B. Reynolds, M. Frank, and A. Halliday (2006), Mechanisms controlling the silicon isotopic compositions of river waters, *Earth Planet. Sci. Lett.*, *249*(3–4), 290–306, doi:10.1016/j.epsl.2006.07.006.

Georg, R. B., A. J. West, D. Vance, K. Newman, and A. N. Halliday (2013), Is the marine osmium isotope record a probe for CO_2 release from sedimentary rocks?, *Earth Planet. Sci. Lett.*, *367*, 28–38, doi:10.1016/j.epsl.2013.02.018.

Girardin, C. A. J., et al. (2010), Net primary productivity allocation and cycling of carbon along a tropical forest elevational transect in the Peruvian Andes, *Global Change Biol.*, *16*(12), 3176–3192, doi:10.1111/j.1365-2486.2010.02235.x.

Godsey, S. E., J. W. Kirchner, and D. W. Clow (2009), Concentration-discharge relationships reflect chemostatic characteristics of US catchments, *Hydrol. Processes*, *23*(13), 1844–1864, doi:10.1002/hyp.7315.

Guinoiseau, D., J. Bouchez, A. Gélabert, P. Louvat, N. Filizola, and M. F. Benedetti (2016), The geochemical filter of large river confluences, *Chem. Geol.*, *441*, 191–203, doi:10.1016/j.chemgeo.2016.08.009.

Hahm, W. J., C. S. Riebe, C. E. Lukens, and S. Araki (2014), Bedrock composition regulates mountain ecosystems and landscape evolution, *Proc. Natl. Acad. Sci. U. S. A.*, *111*(9), 3338–3343, doi:10.1073/pnas.1315667111.

Hartmann, J., N. Moosdorf, R. Lauerwald, M. Hinderer, and A. J. West (2014), Global chemical weathering and associated P-release—The role of lithology, temperature and soil properties, *Chem. Geol.*, *363*, 145–163, doi:10.1016/j.chemgeo.2013.10.025.

Hem, J. D. (1948), Fluctuations in concentration of dissolved solids of some southwestern streams, *Trans. AGU*, *29*(1), 80, doi:10.1029/TR029i001p00080.

Henchiri, S., J. Gaillardet, M. Dellinger, J. Bouchez, and R. G. M. Spencer (2016), Riverine dissolved lithium isotopic signatures in low-relief central Africa and their link to weathering regimes, *Geophys. Res. Lett.*, *43*, 4391–4399, doi:10.1002/2016GL067711.

Herndon, E. M., A. L. Dere, P. L. Sullivan, D. Norris, B. Reynolds, and S. L. Brantley (2015), Landscape heterogeneity drives contrasting concentration-discharge relationships in shale headwater catchments, *Hydrol. Earth Syst. Sci.*, *19*(8), 3333–3347, doi:10.5194/hess-19-3333-2015.

Ibarra, D. E., J. K. Caves, S. Moon, D. L. Thomas, J. Hartmann, C. P. Chamberlain, and K. Maher (2016), Differential weathering of basaltic and granitic catchments from concentration-discharge relationships, *Geochim. Cosmochim. Acta*, *190*, 265–293, doi:10.1016/j.gca.2016.07.006.

Ilina, S. M., S. A. Lapitskiy, Y. V. Alekhin, J. Viers, M. Benedetti, and O. S. Pokrovsky (2016), Speciation, size fractionation and transport of trace elements in the continuum soil Water–Mire–Humic Lake–River–Large Oligotrophic Lake of a Subarctic Watershed, *Aquat. Geochem.*, *22*(1), 65–95, doi:10.1007/s10498-015-9277-8.

INGEMMET (2013), GEOCATMIN Geologia Integrada Por Proyectos Regionales, technical report, Inst. Geol. Minero Metal., Lima.

Jacobson, A. D., J. D. Blum, and L. M. Walter (2002), Reconciling the elemental and Sr isotope composition of Himalayan weathering fluxes: Insights from the carbonate geochemistry of stream waters, *Geochim. Cosmochim. Acta*, *66*(19), 3417–3429, doi:10.1016/S0016-7037(02)00951-1.

Jiann, K. T., P. H. Santschi, and B. J. Presley (2013), Relationships between geochemical parameters (pH, DOC, SPM, EDTA concentrations) and trace metal (Cd, Co, Cu, Fe, Mn, Ni, Pb, Zn) concentrations in river waters of Texas (USA), *Aquat. Geochem.*, *19*(2), 173–193, doi:10.1007/s10498-013-9187-6.

Johnson, N. M., G. E. Likens, F. H. Bormann, D. W. Fisher, and R. S. Pierce (1969), A working model for the variation in stream water chemistry at the Hubbard Brook Experimental Forest, New Hampshire, *Water Resour. Res.*, *5*(6), 1353, doi:10.1029/WR005i006p01353.

Kim, H., J. K. B. Bishop, W. E. Dietrich, and I. Y. Fung (2014), Process dominance shift in solute chemistry as revealed by long-term high-frequency water chemistry observations of groundwater flowing through weathered argillite underlying a steep forested hillslope, *Geochim. Cosmochim. Acta*, *140*, 1–19, doi:10.1016/j.gca.2014.05.011.

Kim, H., W. E. Dietrich, B. M. Thurnhoffer, J. K. B. Bishop, and I. Y. Fung (2017), Controls on solute concentration-discharge relationships revealed by simultaneous hydrochemistry observations of hillslope runoff and stream flow: The importance of critical zone structure, *Water Resour. Res.*, *53*, 1424–1443, doi:10.1002/2016WR019722.

Kirchner, J. W. (2016a), Aggregation in environmental systems—Part 1: Seasonal tracer cycles quantify young water fractions, but not mean transit times, in spatially heterogeneous catchments, *Hydrol. Earth Syst. Sci.*, *20*, 279–297, doi:10.5194/hessd-12-3105-2015.

Kirchner, J. W. (2016b), Aggregation in environmental systems—Part 2: Catchment mean transit times and young water fractions under hydrologic nonstationarity, *Hydrol. Earth Syst. Sci.*, *20*(1), 279–297, doi:10.5194/hess-20-279-2016.

Kirchner, J. W., and C. Neal (2013), Universal fractal scaling in stream chemistry and its implications for solute transport and water quality trend detection, *Proc. Natl. Acad. Sci. U. S. A.*, *110*(30), 12,213–12,218, doi:10.1073/pnas.1304328110.

Kirchner, J. W., P. J. Dillon, and B. D. Lazerte (1993a), Predictability of geochemical buffering and runoff acidification in spatially heterogeneous catchments, *Water Resour. Res.*, *29*(12), 3891–3901, doi:10.1029/93WR02202.

Kirchner, J. W., P. J. Dillon, and B. D. Lazerte (1993b), Separating hydrological and geochemical influences on runoff acidification in spatially heterogeneous catchments, *Water Resour. Res.*, *29*(12), 3903–3916, doi:10.1029/93WR02203.

Kurtz, A. C., F. Lugolobi, and G. Salvucci (2011), Germanium-silicon as a flow path tracer: Application to the Rio Icacos watershed, *Water Resour. Res.*, *47*, W06516, doi:10.1029/2010WR009853.

Lambs, L., A. Horwath, T. Otto, F. Julien, and P. O. Antoine (2012), Isotopic values of the Amazon headwaters in Peru: Comparison of the wet upper Río Madre de Dios watershed with the dry Urubamba-Apurimac river system, *Rapid Commun. Mass Spectrom.*, *26*(7), 775–784, doi:10.1002/rcm.6157.

Li, G., and H. Elderfield (2013), Evolution of carbon cycle over the past 100 million years, *Geochim. Cosmochim. Acta*, *103*, 11–25, doi:10.1016/j.gca.2012.10.014.

Liu, F., M. H. Conklin, and G. D. Shaw (2017), Insights into hydrologic and hydrochemical processes based on concentration-discharge and end-member mixing analyses in the mid-Merced River Basin, Sierra Nevada, California, *Water Resour. Res.*, *53*, 832–850, doi:10.1002/2016WR019437.

Maher, K. (2011), The role of fluid residence time and topographic scales in determining chemical fluxes from landscapes, *Earth Planet. Sci. Lett.*, *312*(1–2), 48–58, doi:10.1016/j.epsl.2011.09.040.

Maher, K., and C. P. Chamberlain (2014), Hydrologic regulation of chemical weathering and the geologic carbon cycle, *Science*, *343*(6178), 1502–1504, doi:10.1126/science.1250770.

Mavromatis, V., A. S. Prokushkin, O. S. Pokrovsky, J. Viers, and M. A. Korets (2014), Magnesium isotopes in permafrost-dominated Central Siberian larch forest watersheds, *Geochim. Cosmochim. Acta*, *147*, 76–89, doi:10.1016/j.gca.2014.10.009.

Meade, R. H. (1996), Contaminants in the Mississippi River, 1987–92, technical report 1133, U.S. Geol. Surv.

Mendívil Echevarría, D., and S. Dávila Manrique (1994), Geología de los cuadrángulos de Cuzco y Livitaca, technical report, Instituto Geológica Nacional, Lima, Peru.

Miller, W. R., and J. I. Drever (1977), Water chemistry of a stream following a storm, Absaroka Mountains, Wyoming, *Bull. Geol. Soc. Am.*, *88*(2), 286–290, doi:10.1130/0016-7606(1977)88 < 286:WCOASF>2.0.CO;2.

Misra, S., and P. N. Froelich (2012), Lithium isotope history of Cenozoic seawater: changes in silicate weathering and reverse weathering., *Science*, *335*(6070), 818–823, doi:10.1126/science.1214697.

Moatar, F., B. W. Abbott, C. Minaudo, F. Curie, and G. Pinay (2017), Elemental properties, hydrology, and biology interact to shape concentration-discharge curves for carbon, nutrients, sediment, and major ions, *Water Resour. Res.*, *53*, 1270–1287, doi:10.1002/2016WR019635.

Moon, S., Y. Huh, J. Qin, and N. van Pho (2007), Chemical weathering in the Hong (Red) River basin: Rates of silicate weathering and their controlling factors, *Geochim. Cosmochim. Acta*, *71*(6), 1411–1430, doi:10.1016/j.gca.2006.12.004.

Moon, S., C. Chamberlain, and G. Hilley (2014), New estimates of silicate weathering rates and their uncertainties in global rivers, *Geochim. Cosmochim. Acta*, *134*, 257–274, doi:10.1016/j.gca.2014.02.033.

Moore, J., A. D. Jacobson, C. Holmden, and D. Craw (2013), Tracking the relationship between mountain uplift, silicate weathering, and long-term CO_2 consumption with Ca isotopes: Southern Alps, New Zealand, *Chem. Geol.*, *341*, 110–127, doi:10.1016/j.chemgeo.2013.01.005.

Moquet, J. S., et al. (2015), Amazon River dissolved load: Temporal dynamics and annual budget from the Andes to the ocean, *Environ. Sci. Pollut. Res.*, *23*, 11,405–11,429, doi:10.1007/s11356-015-5503-6.

Mortlock, R., and P. Froelich (1996), Determination of germanium by isotope dilution-hydride generation inductively coupled plasma mass spectrometry, *Anal. Chim. Acta*, *332*, 277–284.

Mouvet, C., and A. C. M. Bourg (1983), Speciation (including adsorbed species) of copper, lead, nickel and zinc in the Meuse River, Observed results compared to values calculated with a chemical equilibrium computer program, *Water Res.*, *17*(6), 641–649, doi:10.1016/0043-1354(83)90233-6.

Mulholland, D. S., F. Poitrasson, G. R. Boaventura, T. Allard, L. C. Vieira, R. V. Santos, L. Mancini, and P. Seyler (2014), Insights into iron sources and pathways in the Amazon River provided by isotopic and spectroscopic studies, *Geochim. Cosmochim. Acta*, *150*, 142–159, doi:10.1016/j.gca.2014.12.004.

Murnane, R., and R. Stallard (1990), Germanium and silicon in rivers of the Orinoco drainage basin, *Nature*, *344*, 749–752.

Neal, C., and N. Christophersen (1989), Inorganic aluminium-hydrogen ion relationships for acidified streams; the role of water mixing processes, *Sci. Total Environ.*, *80*(2–3), 195–203, doi:10.1016/0048-9697(89)90075-2.

Neal, C., et al. (2013), High-frequency precipitation and stream water quality time series from Plynlimon, Wales: An openly accessible data resource spanning the periodic table, *Hydrol. Processes*, *27*(17), 2531–2539, doi:10.1002/hyp.9814.
O'Connor, D. J. (1976), The concentration of dissolved solids and river flow, *Water Resour. Res.*, *12*(2), 279–294, doi:10.1029/WR012i002p00279.
Peters, N. E., and C. T. Driscoll (1987), Hydrogeologic controls of surface-water chemistry in the Adirondack region of New York State, *Biogeochemistry*, *3*(1–3), 163–180, doi:10.1007/BF02185191.
Peters, N. E., D. A. Burns, and B. T. Aulenbach (2014), Evaluation of high-frequency mean streamwater transit-time estimates using groundwater age and dissolved silica concentrations in a small forested watershed, *Aquat. Geochem.*, *20*(2–3), 183–202, doi:10.1007/s10498-013-9207-6.
Pettine, M., M. Camusso, W. Martinotti, R. Marchetti, R. Passino, and G. Queirazza (1994), Soluble and particulate metals in the Po River: Factors affecting concentrations and partitioning, *Sci. Total Environ.*, *145*(3), 243–265, doi:10.1016/0048-9697(94)90118-X.
Pogge Von Strandmann, P. A. E., J. Forshaw, and D. N. Schmidt (2014), Modern and Cenozoic records of seawater magnesium from foraminiferal Mg isotopes, *Biogeosciences*, *11*(18), 5155–5168, doi:10.5194/bg-11-5155-2014.
Pokrovsky, O. S., J. Schott, and B. Dupré (2006), Trace element fractionation and transport in boreal rivers and soil porewaters of permafrost-dominated basaltic terrain in Central Siberia, *Geochim. Cosmochim. Acta*, *70*(13), 3239–3260, doi:10.1016/j.gca.2006.04.008.
Ponton, C., A. J. West, S. J. Feakins, and V. Galy (2014), Leaf wax biomarkers in transit record river catchment composition, *Geophys. Res. Lett.*, *41*, 6420–6427, doi:10.1002/2014GL061328.
Safran, E. B., P. R. Bierman, R. Aalto, T. Dunne, K. X. Whipple, and M. Caffee (2005), Erosion rates driven by channel network incision in the Bolivian Andes, *Earth Surf. Processes Landforms*, *30*(8), 1007–1024, doi:10.1002/esp.1259.
Saitoh, Y., K. Kuma, Y. Isoda, H. Kuroda, H. Matsuura, T. Wagawa, H. Takata, N. Kobayashi, S. Nagao, and T. Nakatsuka (2008), Processes influencing iron distribution in the coastal waters of the Tsugaru Strait, Japan, *J. Oceanogr.*, *64*(6), 815–830, doi:10.1007/s10872-008-0068-3.
Shand, P., A. H. Haria, C. Neal, K. J. Griffiths, D. C. Gooddy, A. J. Dixon, T. Hill, D. K. Buckley, and J. E. Cunningham (2005), Hydrochemical heterogeneity in an upland catchment: Further characterisation of the spatial, temporal and depth variations in soils, streams and groundwaters of the Plynlimon forested catchment, Wales, *Hydrol. Earth Syst. Sci.*, *9*(6), 621–644, doi:10.5194/hess-9-621-2005.
Shiller, A. M. (1997), Dissolved trace elements in the Mississippi River: Seasonal, interannual, and decadal variability, *Geochim. Cosmochim. Acta*, *61*(20), 4321–4330, doi:10.1016/S0016-7037(97)00245-7.
Shiller, A. M., and E. Boyle (1985), Dissolved zinc in rivers, *Nature*, *317*(6032), 49–52, doi:10.1038/317049a0.
Shiller, A. M., and L. Mao (2000), Dissolved vanadium in rivers: Effects of silicate weathering, *Chem. Geol.*, *165*(1–2), 13–22, doi:10.1016/S0009-2541(99)00160-6.
Stallard, R., and J. Edmond (1983), Geochemistry of the Amazon: 2. The influence of geology and weathering environment on the dissolved load, *J. Geophys. Res.*, *88*(C14), 9671–9688.
Stefánsson, A., and S. R. Gíslason (2001), Chemical weathering of basalts, southwest Iceland: Effect of rock crystallinity and secondary minerals on chemical fluxes to the ocean, *Am. J. Sci.*, *301*(6), 513–556, doi:10.2475/ajs.301.6.513.
Tipper, E. T., M. J. Bickle, A. Galy, A. J. West, C. Pomiès, and H. J. Chapman (2006), The short term climatic sensitivity of carbonate and silicate weathering fluxes: Insight from seasonal variations in river chemistry, *Geochim. Cosmochim. Acta*, *70*(11), 2737–2754, doi:10.1016/j.gca.2006.03.005.
Tipper, E. T., D. Calmels, J. Gaillardet, P. Louvat, F. Capmas, and B. Dubacq (2012), Positive correlation between Li and Mg isotope ratios in the river waters of the Mackenzie Basin challenges the interpretation of apparent isotopic fractionation during weathering, *Earth Planet. Sci. Lett.*, *333–334*, 35–45, doi:10.1016/j.epsl.2012.04.023.
Torres, M. A., A. J. West, and K. E. Clark (2015), Geomorphic regime modulates hydrologic control of chemical weathering in the Andes-Amazon, *Geochim. Cosmochim. Acta*, *166*, 105–128, doi:10.1016/j.gca.2015.06.007.
Torres, M. A., A. J. West, K. E. Clark, G. Paris, J. Bouchez, C. Ponton, S. J. Feakins, V. Galy, and J. F. Adkins (2016), The acid and alkalinity budgets of weathering in the Andes-Amazon system: Insights into the erosional control of global biogeochemical cycles, *Earth Planet. Sci. Lett.*, *450*, 381–391, doi:10.1016/j.epsl.2016.06.012.
Torres, M. A., J. J. Baronas, K. E. Clark, S. J. Feakins, and A. J. West (2017), Mixing as a driver of temporal variations in river hydrochemistry: 1. Insights from conservative tracers in the Andes-Amazon transition, *Water Resour. Res.*, *53*, doi:10.1002/2016WR019733.
Trostle, K., J. Runyon, M. Pohlmann, S. Redfield, J. Pelletier, J. McIntosh, and J. Chorover (2016), Colloids and organic matter complexation control trace metal concentration-discharge relationships in Marshall Gulch Stream waters, *Water Resour. Res.*, *52*, 7931–7944, doi:10.1002/2016WR019072.
Vargas Vilchez, L., and A. Hipolito Romero (1998), Geología de los cuadrángulos de Río Pinquén, Pilcopata y Chontachaca, technical report (25t-27t), Inst. Geol. Nac., Lima.
Viers, J., B. Dupré, M. Polvé, J. Schott, J.-L. Dandurand, and J.-J. Braun (1997), Chemical weathering in the drainage basin of a tropical watershed (Nsimi-Zoetele site, Cameroon): Comparison between organic-poor and organic-rich waters, *Chem. Geol.*, *140*, 181–206.
Voss, B. M., et al. (2014), Tracing river chemistry in space and time: Dissolved inorganic constituents of the Fraser River, Canada, *Geochim. Cosmochim. Acta*, *124*, 283–308, doi:10.1016/j.gca.2013.09.006.
Walker, J. C., P. Hays, and J. Kasting (1981), A negative feedback mechanism for the long-term stabilization of Earth's surface temperature, *J. Geophys. Res.*, *86*(C10), 9776–9782, doi:10.1029/JC086iC10p09776.
Walling, D. E., and B. W. Webb (1980), The spatial dimension in the interpretation of stream solute behaviour, *J. Hydrol.*, *47*(1–2), 129–149, doi:10.1016/0022-1694(80)90052-9.
West, A. J. (2012), Thickness of the chemical weathering zone and implications for erosional and climatic drivers of weathering and for carbon-cycle feedbacks, *Geology*, *40*(9), 811–814, doi:10.1130/G33041.1.
Yang, M., and S. A. Sañudo-Wilhelmy (1998), Cadmium and manganese distributions in the Hudson River estuary: Interannual and seasonal variability, *Earth Planet. Sci. Lett.*, *160*(3–4), 403–418, doi:10.1016/S0012-821X(98)00100-9.
Zimmermann, M., J. Leifeld, F. Conen, M. I. Bird, and P. Meir (2012), Can composition and physical protection of soil organic matter explain soil respiration temperature sensitivity?, *Biogeochemistry*, *107*(1–3), 423–436, doi:10.1007/s10533-010-9562-y.